THE ALUMINIUM ELECTRODE POTENTIAL

A thesis presented for the degree of
Doctor of Philosophy in Chemical Engineering
in the University of Canterbury
Christchurch, New Zealand

by

W. B. EARL

1965

ACKNOWLEDGMENTS

I would like to express my thanks to Dr T. Hagyard, who supervised this work, for his time, assistance and enthusiasm over the last few years. A number of members of this department have helped in many ways and I am most grateful to them.

Thanks are also due to the New Zealand Research Fund Committee whose financial assistance enabled the purchase of equipment necessary in this research.

CONTENTS

ABSTRACT

A square wave current technique has been used to obtain the cathodic overvoltage parameters for hydrogen evolution on aluminium but was found inadequate by itself for determining the anodic parameters for aluminium dissolution, mainly because of the complicating effects of solution IR drop. A method was developed, however, for the determination of α_a and the ratio C/i_{oa} from the analysis of the initial potential fall in the 20 μsecs during and just after cutting. By combining these results with the square wave results, the IR drop and i_{oa} were found and hence C could be obtained from C/i_{oa}.

It is shown that the potential time behaviour in the first few milliseconds on freshly exposing an aluminium surface to aqueous salt solutions cannot be explained simply in terms of the electrode kinetic parameters applicable to the existing polyelectrode. The observations have been accounted for using the polyelectrode parameters if the ratio of cathodic to anodic area changes rapidly (T.C. 0.2 ms) with time after an effective delay of approximately 20 μsecs.

1. INTRODUCTION

1.1 General

It has been observed by at least one author[1] for many metals (Be, Mg, Al, Nb, Cr, and others) and by a number of authors[2,3,4] for Al, that the electrode potentials of these metals in a number of solutions can be made 300-1000 mV more negative by cleaning the electrode surface, this meaning in most cases merely the removal of the naturally occurring oxide film. Morize and Lacombe[3] obtained a potential of -0.9v in 3% NaCl solution for an aluminium electrode cleaned in an air- and water-free environment. Some years later, one of the same authors[5] obtained a potential of -1.3v in the same solution by presumably taking more care in oxygen elimination. More recent workers, e.g. Ergang, Masing, and Mohling[6] have obtained even more negative potentials -1.5v in a 0.1% NaCl solution. Even in these cases, where especially rigorous attempts were made to eliminate any oxide films present, the electrodes would certainly be polyelectrodes composed of aluminium anodes polarised by polarised hydrogen cathodes. In such cases the presence of oxide films prevents investigation of the processes occurring on a clean aluminium electrode.

1.2 Review of Previous Work in this Field

It would seem in fact that it was not until the work of Hagyard and Williams[7] that potentials of an aluminium electrode free from oxide films and competing reactions were obtained very close to the theoretical reversible potential of aluminium.

In this work an insulated aluminium electrode was cut in a very short time under solution and the potential of the freshly-cut surface

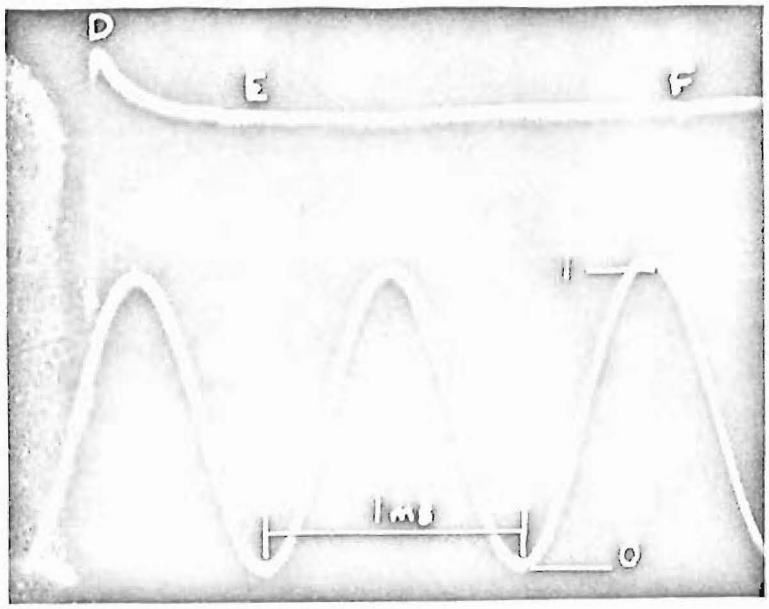

Fig. 1. Potential versus time trace for an unpolarised aluminium electrode. D, peak potential; E-F mixed potential. O zero volts on N.Calomel scale. 1 one Weston cell negative of O.

with respect to the electrolyte was measured oscillographically. It was found that the peak potential (see Fig. 1 - Fig. 3 in ref. 7) was affected by aluminium ion concentration but not pH and that the mixed potential was affected by pH but not by aluminium ion concentration, thus showing that the electrode was anodically active at the peak, and although of necessity anodically as well as cathodically active at the mixed potential, apparently cathodically controlled. Later work[8] used the observation above, that the peak potential behaved solely as an aluminium electrode to obtain anodic polarisation parameters i_o and α for aluminium dissolution. Further justification[9] for this is discussed in a later section. It was believed at this stage that anodic parameters could be obtained in the very short times, 20 μsec, required to reach the peak potential because the hydrogen evolution process was thought

to be too slow to affect the anodic measurement made in these times. For the measurement of hydrogen discharge parameters on aluminium another property of the system had to be used because normally both processes would be fully established by this time. When an aluminium electrode is polarised cathodically to a potential much more negative than the aluminium reversible potential in a given solution, there can be no anodic dissolution of aluminium. Thus by polarising the newly-cut surface with current densities high enough to produce potentials appreciably more negative than the peak potential this condition existed, and the cathodic polarisation results so obtained refer to an aluminium surface, none of which was anodic, i.e. to a surface wholly cathodic on which the only feasible process occurring was the discharge of hydrogen ions. Potassium ion, the other cation in solution, was effectively prohibited from discharging because, firstly, if potassium were discharged then it would be expected to exhibit unit activity as potassium is substantially insoluble in aluminium[10], and secondly, the most polarised electrode potential was still some 0.5 volts more positive than the expected reversible potential for a potassium electrode in this solution.

By extrapolating the anodic and cathodic Tafel lines so obtained to the measured mixed potential at zero external current it was found that the current density on the cathodic area at this potential must have been about 200 times less than the current density on the anodic area at the same potential. However, the internal currents flowing between anode and cathode for an unpolarised electrode must of necessity be equal. This meant that at the mixed potential the cathodic area must be ca. 200 times the anodic area; thus the area must change from presumably being all anodic at the peak potential to being predominantly cathodic at the

mixed potential.

Attempts have been made in this thesis to answer some of the questions arising from this work, e.g. what is the cause of the relatively slow fall from peak to mixed potential? Does the electrode function start to change from anodic to cathodic right from the time of cutting, only after reaching the peak, quickly at the peak, or slowly during the decay to the mixed potential?

A number of methods has been developed for the study of fast electrode charge transfer reactions, a major objective being the elimination of diffusion controlled effects. A.C. methods, first used by Frumkin et al[11] and later extensively developed by Randles[12], Gerischer[13], and Delahay[14], are very useful in this field but not applicable in the case of the present work because they require some minutes at best, balancing bridges, etc, and measurements in this work had to be made within a few milliseconds. Of the three remaining methods it was decided to use a current step method, discussed in the next section, for the present work; potential step methods[15,16] and the newer method of Faradaic rectification[17] were more difficult experimentally and did not appear to offer any advantages over a current step method at the present time.

Thus a current step method employing a square wave loading current was used to overcome a number of disadvantages present with the static polarisation method used in the previous work. This, as is shown in a later section, enabled the roughness of the cut surface and its actual area to be eliminated as a variable in the determination of α, the transfer coefficient. Although the apparent area of the cut must still be used in the determination of i_0, at least a consistent surface is

obtained within a run. Besides reducing considerably the effect of roughness as outlined above, the square wave technique could give twice as much information from each run and it was hoped more insight into the basic kinetics of the electrode reactions.

1.3 Current Step or Square Wave Current Methods

Current step methods for the elucidation of electrode kinetics have been treated by a number of authors[18,19,20,21,22]. Sand[18] and Karaoglanoff[19], however, did not take into account the capacitive portion of the current used in charging or discharging the electrical double layer, which is necessary in many cases and certainly in this work. The general treatment of current step methods encounters serious mathematical difficulties. Rojter, Juza and Polujan[20] have obtained a general but very complex solution for the case where the transfer coefficient, α, is 0.5 and no concentration changes occur at the electrode. Berzins and Delahay[23] have published a more general treatment restricted, however, to small amplitudes of the voltage response and to symmetrical (viz. time equal for each flat) square waves. Wijnen and Smit[21] have presented a 'cyclic current step' method extending the theory of Berzins and Delahay to the case of asymmetrical square waves. After their rigorous analysis it was unfortunate that they introduced the usual restriction of small values of overvoltage to enable them to get a solution to their equations, e.g. the error arising from this restriction is 200% for an overvoltage of 100 mV, ca. 1.8% at 10 mV.

In the case of the present work it is not possible to obtain directly the electrokinetic parameters for the discharge of hydrogen on aluminium at anything less than ca. -1.5 volts overvoltage because the

electrode is really a polyelectrode at potentials more positive than this, viz. an anode for aluminium dissolution as well as a cathode for hydrogen discharge.

2. CONSIDERATION OF ELECTRODE KINETICS INVOLVED

When a constant current density is suddenly applied to an electrode it can be considered to divide into two components. The first, ic, is used for charging the electrical double layer at the electrode solution interface, the second part, i_f, brings about transfer of charge across the double layer, either as ions from the metal to solution or vice versa, in the case of metal dissolution, or as ions from the solution to the metal or electrons from the metal to the solution, in the case of gas discharge. In all cases we have:

$$i = ic + i_f \qquad (1)$$

Consider only a cathodic reaction occurring on the electrode. The capacitive current density ic rapidly decreases with time as i is constant. If i_{fc} is controlled solely by the charge transfer process then

$$i_{fc} = i_{oc}\left(e^{-\frac{\beta_c nF\eta_c}{RT}} - e^{\frac{(1-\beta_c)nF\eta_c}{RT}}\right) \quad \text{(ref. 24)} \qquad (2)$$

and thus

$$i = -C\frac{d\eta_c}{dt} + i_{oc}\left(e^{-\frac{\beta_c nF\eta_c}{RT}} - e^{\frac{(1-\beta_c)nF\eta_c}{RT}}\right) \qquad (3)$$

where C = double layer capacity (F/cm^2)

i_{oc} = exchange current for the charge transfer controlled reaction (cathodic) ($amps/cm^2$)

β_c = cathodic electron transfer coefficient, $0 < \beta_c < 1$

n = number of electrons transferred in the cathodic rate controlling process

η_c = cathodic overvoltage = $V - E_{oc}$ (volts)

V = potential of the electrode w.r.t. say H_2 electrode (volts)

E_{oc} = reversible potential of the electrode w.r.t. the same electrode as V (volts)

$\mathcal{R}$, F, T have their usual significance.

Because E_{oc} is constant, then a linear relationship exists between η_c and V and therefore

$$\frac{d\eta_c}{dt} = \frac{dV}{dt} \qquad (4)$$

If now an anodic process is also occurring on the electrode we have a polyelectrode (generally so called; possibly better called a di-electrode). Assuming that this reaction is also charge transfer controlled, then its current density is given by an expression analogous to eqn 2, viz:

$$i_{fa} = i_{oa}\left(e^{-\frac{\beta_a zF\eta_a}{\mathcal{R}T}} - e^{\frac{(1-\beta_a)zF\eta_a}{\mathcal{R}T}}\right) \qquad (5)$$

where i_{oa} = exchange current for the anodic reaction

β_a = anodic electron transfer coefficient, $0 < \beta_a < 1$

z = number of electrons transferred in anodic rate controlling process

η_a = the anodic overvoltage = $V - E_{oa}$

E_{oa} = reversible potential of the anodic reaction, cf. E_{oc}

We thus have for a polarised polyelectrode

$$i = -C\frac{dV}{dt} + i_{oc}\left(e^{-\frac{\beta_c nF\eta_c}{\mathcal{R}T}} - e^{\frac{(1-\beta_c)nF\eta_c}{\mathcal{R}T}}\right) + i_{oa}\left(e^{-\frac{\beta_a zF\eta_a}{\mathcal{R}T}} - e^{\frac{(1-\beta_a)zF\eta_a}{\mathcal{R}T}}\right)$$

i.e. $$i = -C\frac{dV}{dt} + i_{fc} + i_{fa} \qquad (6)$$

assuming that the whole of the electrode area is active both anodically and cathodically, each function occurring as if the other were not present. (If i were negative this would signify anodic loading.)

In earlier work in this field, discussed in a previous section (1.2), the concept of discrete anodic and cathodic areas on the electrode was introduced to explain the observations made. This concept is expressed most concisely as the cathodic to anodic 'area ratio' and is referred to hereafter as area ratio.

Now, when the anodic and cathodic functions are not concurrent on the same surface, eqn 5 becomes

$$i = C\frac{dV}{dt} + \frac{r}{1+r} i_{fc} + \frac{1}{1+r} i_{fa} \qquad (7)$$

where $\frac{r}{1+r}$ = cathodic proportion of the total surface (cm^2/cm^2)

$\frac{1}{1+r}$ = anodic proportion of the total surface (cm^2/cm^2)

r = cathodic to anodic area ratio

Unfortunately, completely general analytical solutions of eqns 3, 6 and 7 are not known. Rojter et al[20] have obtained a very complicated solution to eqn 3 for the case $\beta = 0.5$ and $n = 1$. More recently, Karasyk, Law and Linford[25] have extended this to cases where $n = 2$ and 3. For one process alone (eqn 3) a solution can be obtained analytically by ignoring the contributions of the reverse charge transfer process. This is a close approximation if used at potentials sufficiently far from the reversible potential (as is done in section 4.2.3). For two processes (eqn 7) and/or in the region of a reversible potential it is necessary to use numerical methods for solution. To accomplish this economically, a 1620 computer program was written using a Runge-Kutta method[26] for integrating the required equations. This program is

detailed in Appendix 8.1 and referred to hereafter as Program I.

2.1 The Peak Potential Problem

It can be proved (see Appendix 8.2) that it is not possible to obtain a peak potential (overshoot in electronic terminology) in the solution of eqns 3 and 7 for a step change in loading current, i, if all the overvoltage parameters (i_{oa}, i_{oc}, α_a, α_c) including the area ratio, r, are constant with time. It is possible to obtain overshoot if the area ratio alone changes with time and the rest of the parameters remain constant as shown below.

Assume for a start that the basic parameters (i_o's and α's) do not change with time and that the area ratio, r, changes in, say, an exponential manner. Fig. 2 shows plots of area ratio, r, versus time; r changing exponentially from zero to its final value with three different arbitrary time constants: 0.2 ms, 2 ms and 10 ms.

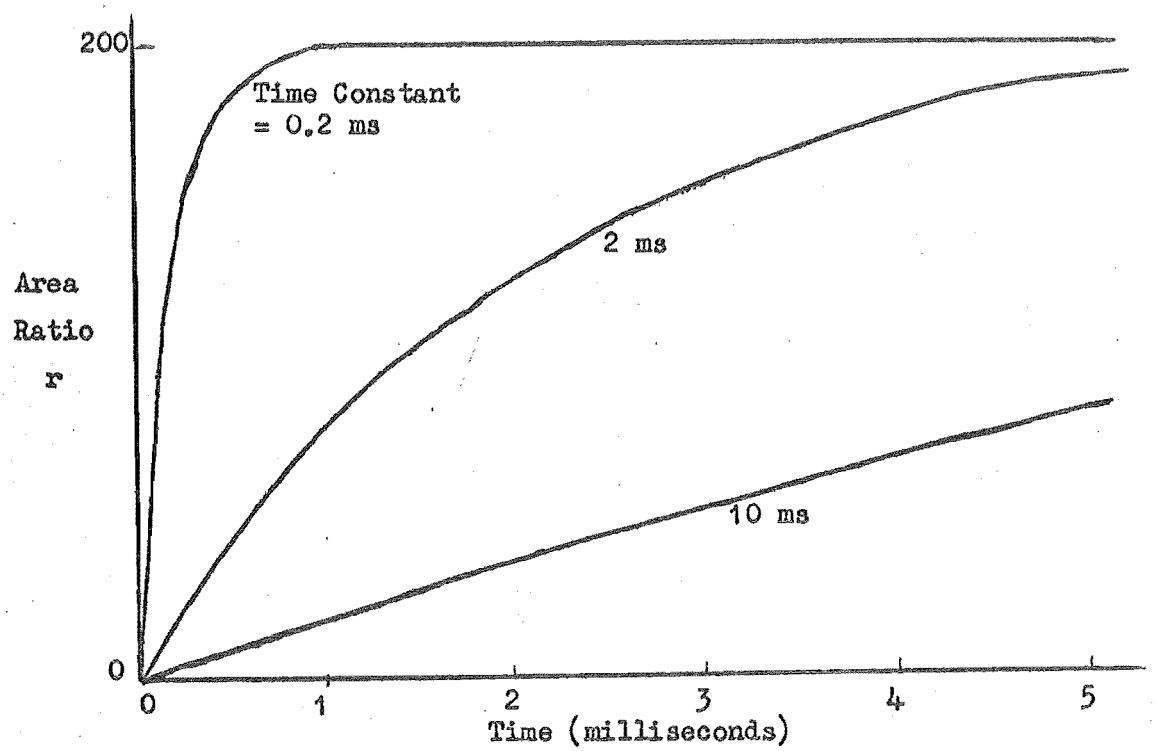

Fig. 2. Arbitrary Exponential Area Ratio v Time Curves

Fig. 3 shows a typical no-load curve (a) obtained experimentally, together with various theoretical curves obtained by solving eqn 7 (with the aid of Program I) using the above assumption concerning area ratio and the values of the anodic and cathodic parameters (i_o's and α's) from previous work[8]. These curves show how easily overshoot is suppressed. Note that a slow area changeover (e.g. 10 ms T.C.) gives a more negative peak potential but a much slower return to the mixed potential; a faster changeover, a faster return to the mixed potential but a suppressed peak.

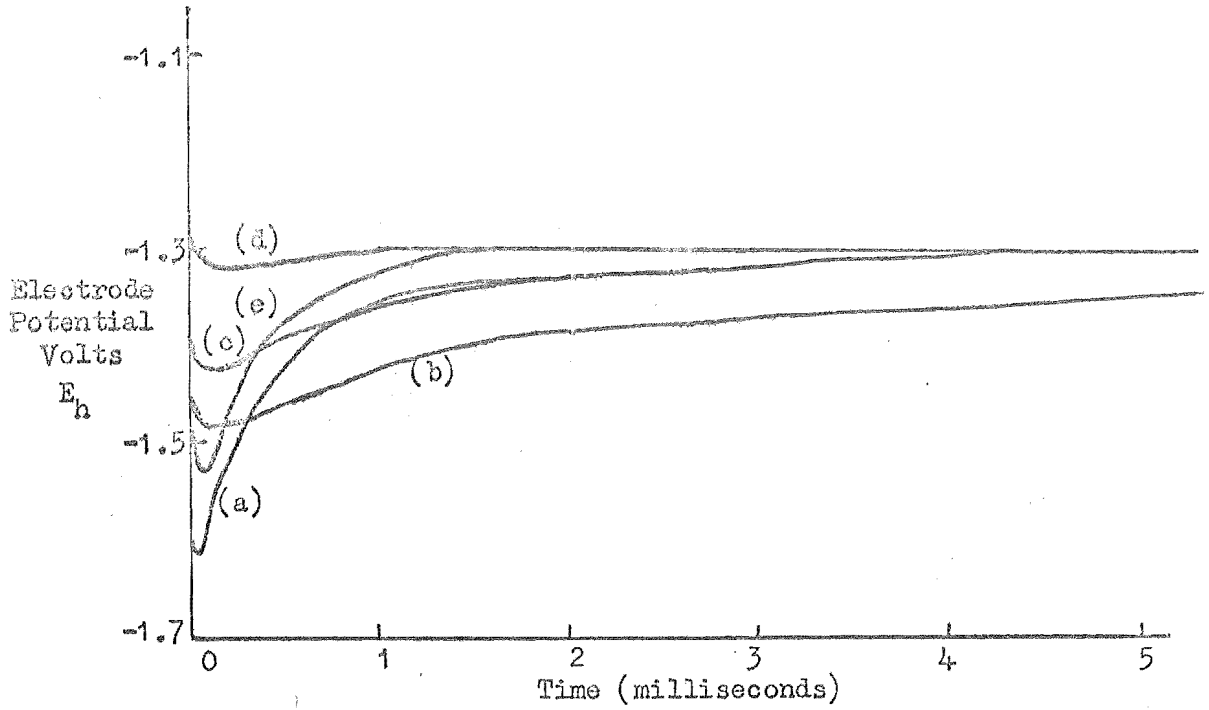

Fig. 3. Electrode Potential v Time Curves.
(a) Observed experimental curve;
(b),(c),(d) Theoretical curves using kinetic parameters from ref. 8
viz. $i_{oa} = 6.3 \times 10^{-4}$ amps/cm^2 $\alpha_a = 0.369$
$i_{oc} = 3.2 \times 10^{-7}$ amps/cm^2 $\alpha_c = 0.188$
and area ratio changeover as shown in Fig. 2. T.C.'s 10, 2, and 0.2 ms respectively.
(e) as for (d) except for initial delay of 100 µsec before area changeover starts.

This suggests, bearing in mind the above assumptions, that a peak potential as is observed (see (a) Fig. 3) can be obtained only if there is effectively a delay in the initiation of the cathodic process and then in a short time thereafter most of the area becomes cathodic with very little active anodic area. The computed trace resulting from such a delay is also shown in Fig. 3, curve (e). Such a delay in the onset of spontaneous hydrogen ion discharge on electronegative metals is postulated from atomic theory by Bass[27] and it would appear that Hagyard's and Williams' observations were the first in which this phenomenon has been experimentally recorded.

Although the explanation above can account for overshoot, the initial shape of the curve as observed does not agree with that calculated, thus suggesting that the anodic parameters previously obtained are not very close to the true values. For this reason further simulation and discussion is postponed until after the cathodic and anodic parameters have been redetermined by the square wave current method mentioned earlier.

3. EXPERIMENTAL

The experimental techniques used in this research were very similar to those used in earlier work in this department under Dr Hagyard, with the exception of a few points mentioned later in this section. In the main they consist of measuring oscillographically the potential of a freshly-cut aluminium surface exposed to an electrolyte solution.

Fig. 4 shows a diagrammatic layout of the main equipment, all, except the oscilloscope and signal or pulse generator, being placed inside an earthed screening cabinet to minimise electrostatic and magnetic effects on the circuitry involved.

All potentials are on the hydrogen scale unless otherwise qualified.

3.1 Voltage Measuring Equipment

A high-speed cathode follower (rise time 0.1 μsec, input impedance >5 MΩ) (circuit diagram Fig. 5) used in earlier measurements in this work was connected to a Cossor 1065 pulse oscilloscope for potential measurements.

Later measurements were made without a cathode follower using a Tektronix 535A oscilloscope with type H amplifier, this having slightly lower but satisfactory input impedance (1 MΩ) and higher speed response (rise time .023 μs).

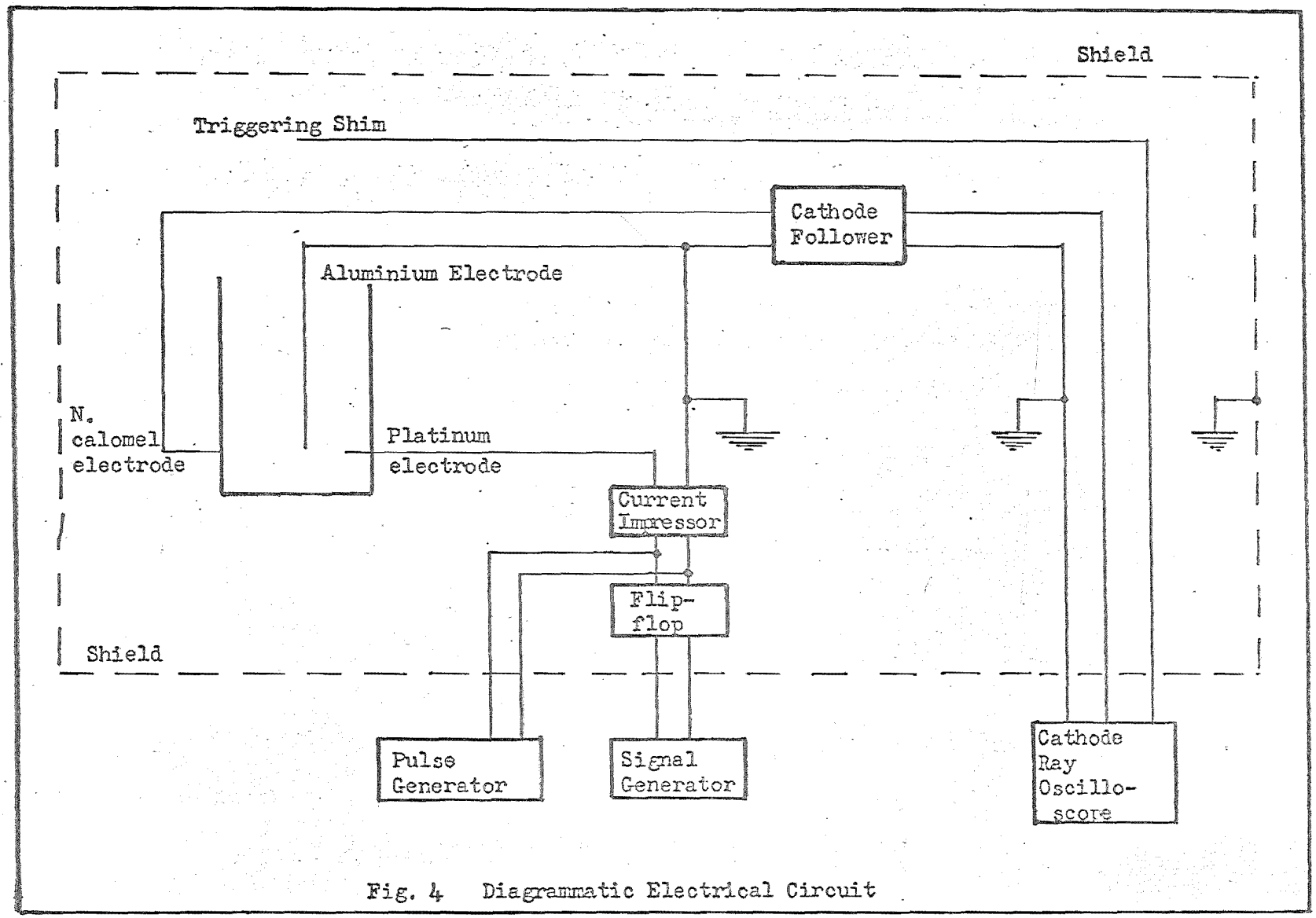

Fig. 4 Diagrammatic Electrical Circuit

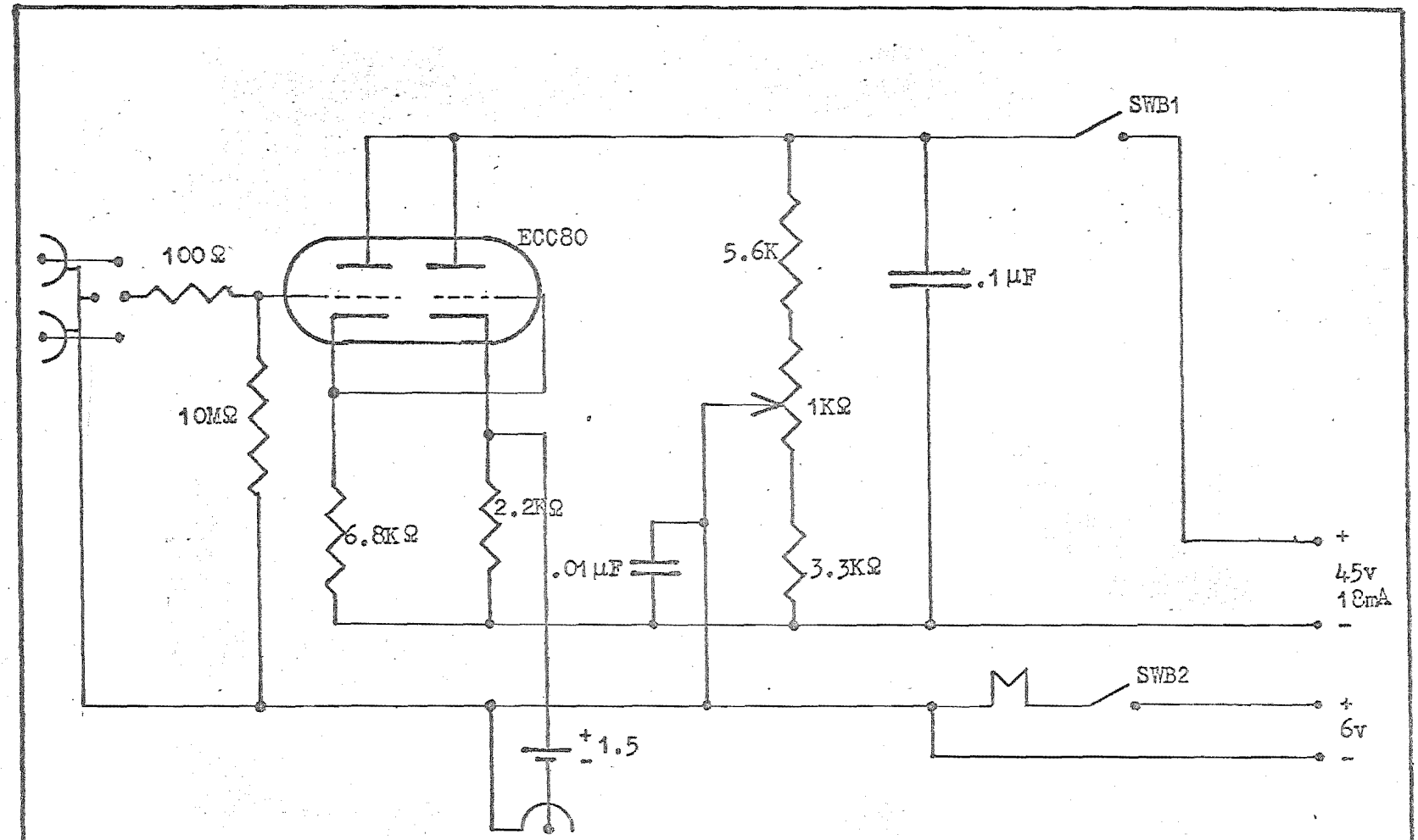

Fig. 5 Cathode Follower Circuit

3.2 Constant Current Control

A current impressor of more advanced design (circuit diagram Fig. 6) but of similar principle to that used in earlier work[8] was developed to enable loads to be applied smoothly variable from cathodic to anodic.

For square wave work it was thus possible to apply a square wave whose average current was zero, i.e. square pulses alternately cathodic and anodic.

3.3 Square Wave Generation

For the earlier measurements a flip-flop circuit (Fig. 7) was used to obtain a square voltage wave (rise and fall times ca. 0.1 μsec) from the roughly square wave output of an "Advance" audio signal generator. The flip-flop was connected to the current impressor thus producing a square current wave which was used in the early part of this work.

For later measurements a G.R. pulse generator (rise time 0.010 μsec) was used, this having three main advantages over the signal generator flip-flop combination; these were (1) the pulse generator could be connected to the current impressor directly thus making the flip-flop unnecessary, (2) the square wave amplitude could be varied smoothly and easily (not possible with flip-flop where discrete changes in amplitude had to be made), and (3) the larger frequency range of the pulse generator compared with the audio oscillator (300 kc v 50 kc). This latter aspect was essential in making anodic square wave measurements.

3.4 Electrodes

Most electrodes were made from aluminium with the following composition:

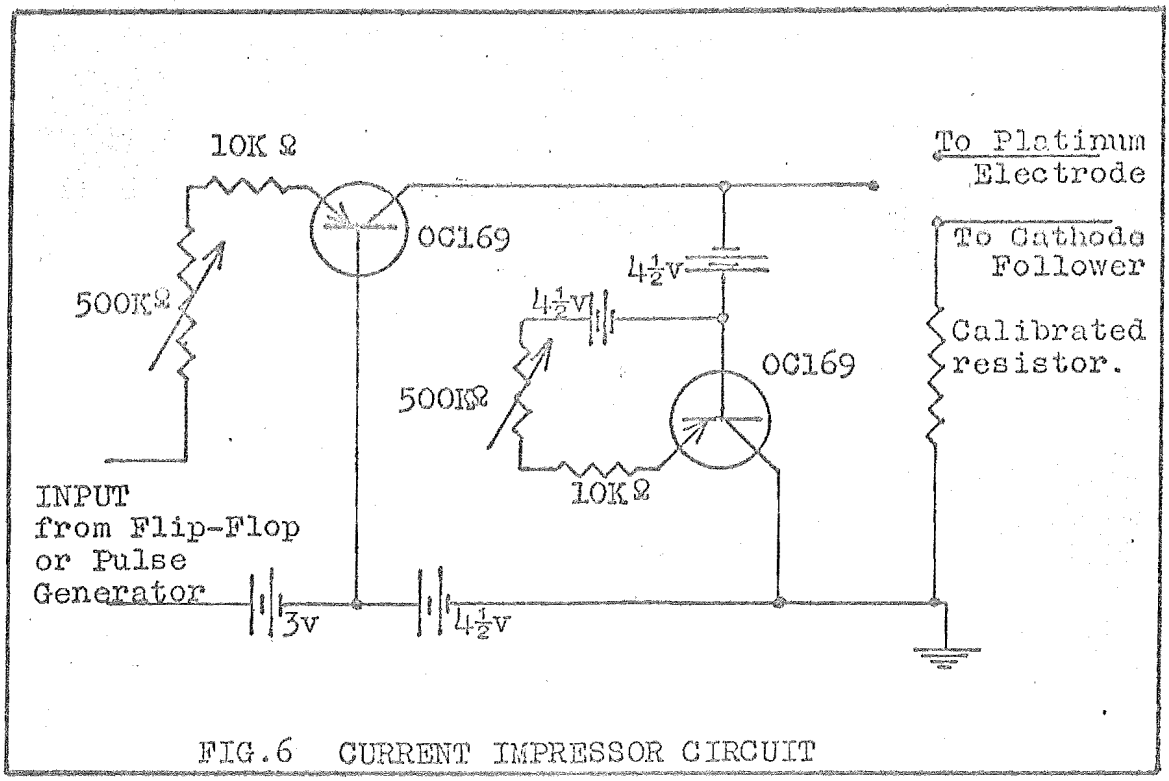

FIG.6 CURRENT IMPRESSOR CIRCUIT

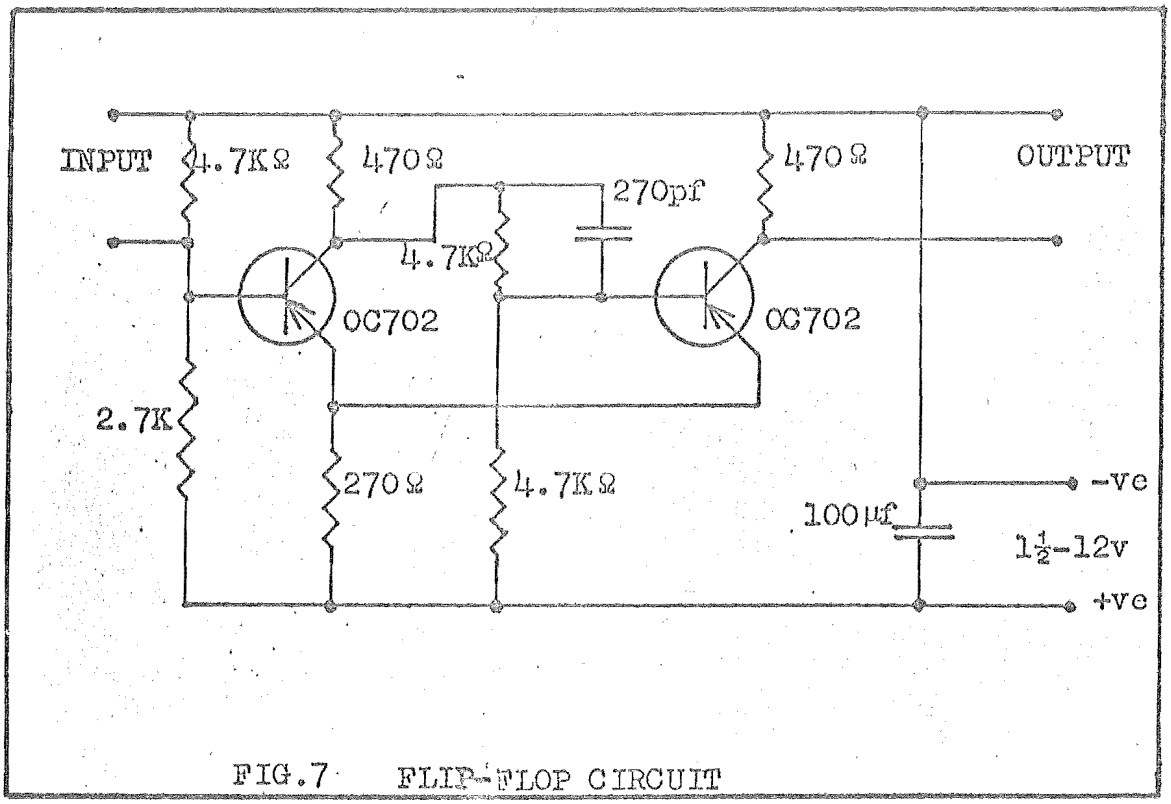

FIG.7 FLIP-FLOP CIRCUIT

Al	99.99% min.	
Si	.0023 min.	.0040 max.
Fe	.0020 "	.0030 max.
Cu	.0020 "	.0025 "

which is the same as that used in previous work in this field[7,8], but a number of runs were made using other grades: one (A) a super pure aluminium, the other (B) a commercial grade.

A 99.9995% Al

B 99.6% Al

to determine the significance of impurities in the aluminium on the measurements made.

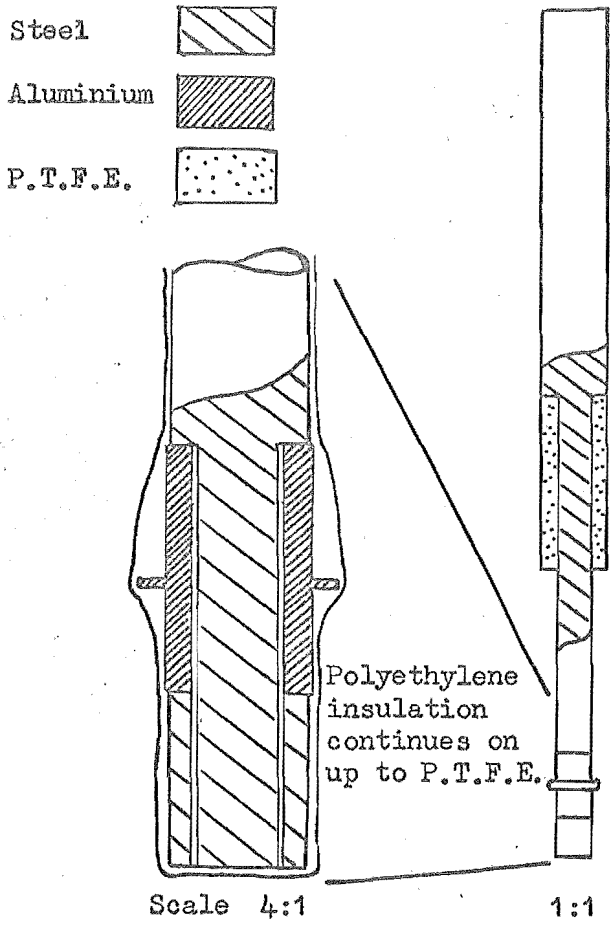

Fig. 8. Construction detail of composite electrode.

The earlier runs used $\frac{1}{4}$" all aluminium rods as used previously, but it was found better to use a steel composite electrode (after Watson[28]) as shown in Fig. 8 especially when using the super pure grade (A) which was very soft and not obtainable as straight rods.

The reference electrode used in all cases was a normal calomel electrode connected to the cell through a salt bridge and cellophane membrane as in previous work[7,8].

The loading electrode used in all loaded runs was a platinum auxiliary electrode as used before[8].

3.5 Electrolyte Solutions

All electrolyte solutions were prepared from "Analar" reagents and de-ionised water. It was not considered necessary to pre-electrolyse or in any other way specially prepare solutions. A quick calculation shows that even at the maximum impurity concentration possible in the solutions the time taken for say 1/1000 of a monolayer of low hydrogen overvoltage impurities to arrive at the surface by diffusion is many times greater than the total times involved in the experimental runs. Perhaps more conclusive proof of sufficient solution purity is that obtained by Watson[28] where he showed that even with low hydrogen overvoltage, solution impurity increased to many times that normally present, no observable effect was obtainable even after times 100 times longer than those used in these runs.

4. RESULTS AND DISCUSSION

4.1 Measurement of Square Wave Polarisation Currents

It is obviously not possible to measure the value of the current for each flat of a square wave current source with a meter. In these experiments this current was obtained by applying the current impressor output to a previously calibrated resistor (see Fig. 6) and observing the resulting voltage across this resistor oscillographically.

Fig. 9(a) shows an oscillograph trace (trace A) obtained in measuring a typical anodic square wave, Fig. 9(b) a cathodic square wave current (trace B). Traces 0, -1 and -2 were voltage calibration lines placed there by manual triggering just prior to A. 0 was at zero volts (i.e. earthed condition), -1 one, and -2 two Weston cells negative with respect to 0.

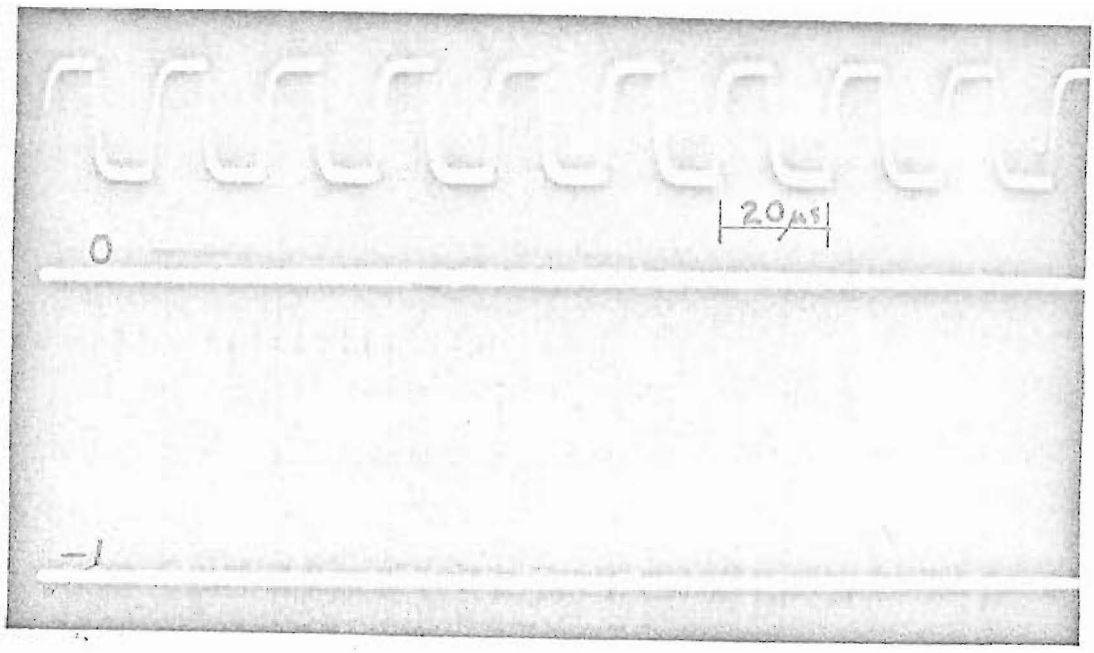

Fig. 9(a) Anodic square wave current measurement.

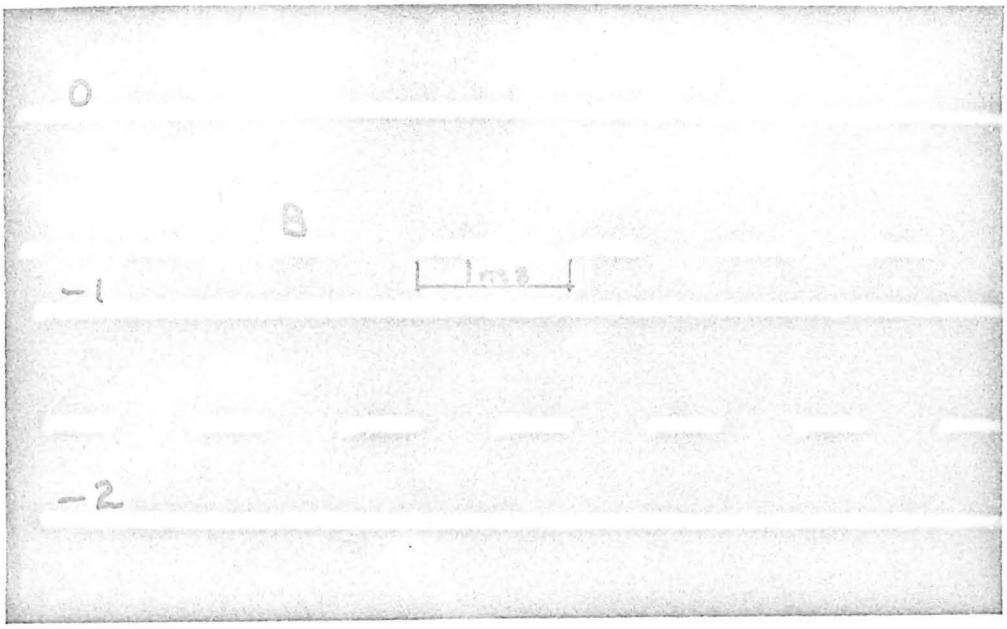

Fig. 9(b) Cathodic square wave current measurement.

A measurement such as the one described above was made just before every square wave loaded run made, the circuitry of the current impressor (Fig. 6) ensuring that the current as set remained constant for the run.

4.2 Anodic Measurements in Chloride Solution

All anodically polarised square wave potential measurements were made within the first fifty microseconds after cutting. The use of these potential flats (some microseconds long) as anodically polarised equilibrium potentials is justified elsewhere[29], but to reiterate very briefly: unpolarised aluminium electrode potentials in this region are -1.65 v[7,8] compared with the calculated E_o = -1.67v quoted by Latimer[30]. Latimer's value refers, of course, to unit aluminium ion activity but has not been confirmed experimentally. Also the activity of the

aluminium ion in these[7,8] solutions is not known. The agreement seems reasonable for the present purposes. Additional justification for these measurements is afforded by similar high-speed measurements made by Chapman[9]. In this work 10-30 μs values of the potential of cadmium in cadmium chloride were compared with values obtained by standard static potentiometric methods. Agreement to about 10 mv was found.

4.2.1 Anodic Square Wave Measurements

1N.KCl + 1/1000 N.$AlCl_3$, pH 3.2 solution was used throughout, the aluminium ion being present so that the reversible potential of the aluminium electrode would be defined. A typical, square wave current, anodically-polarised electrode potential trace is shown in Fig. 10.

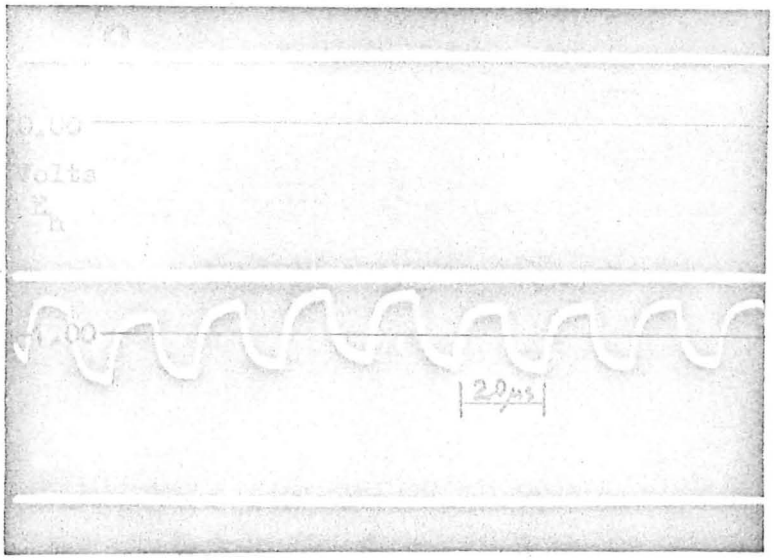

Fig. 10. Anodically polarised electrode potential. 0 is zero volts on N.calomel scale.

The electrode potential trace is with respect to a normal calomel electrode.

From the potentials and current densities so obtained, α and i_o for the anodic process can be obtained as below.

Eqn 6 (p. 7) reverts to eqn 5, viz:

$$i = i_{oa}\left(e^{-\frac{\beta_a z F \eta_a}{RT}} - e^{\frac{(1-\beta_a) z F \eta_a}{RT}}\right) \qquad (5)$$

at steady state and when only the anodic process is occurring on the electrode. When the polarisation is greater than 100 mv this equation can be simplified further to

$$i = -i_{oa} e^{\frac{(1-\beta_a)zF\eta_a}{RT}} \qquad (8)$$

for anodic polarisation and expressed in the more conventional form of Tafel's equation

$$\eta_a = \frac{RT}{\alpha_a F} \ln \frac{1}{i_{oa}} \qquad (9)$$

where $\alpha = (1-\beta_a)z$

(i is negative by convention for anodic polarisation.)

Thus for one flat of the polarisation square wave

$$\eta_{a1} = \frac{RT}{\alpha F} \ln \frac{i_1}{i_{oa}} \qquad (10)$$

for the other flat

$$\eta_{a2} = \frac{RT}{\alpha F} \ln \frac{i_2}{i_{oa}} \qquad (11)$$

Subtracting 11 from 10 and rearranging gives the transfer coefficient

$$\alpha = \frac{RT}{F} \frac{\ln i_1/i_2}{\eta_1 - \eta_2} \qquad (12)$$

As the electrode area only enters into the calculation of the current densities i_1 and i_2, and the ratio of i_1/i_2 into the calculation of α, the electrode area cannot affect the calculation of α. Thus only the ratio of impressed currents need be used in the calculation of α. This means that the surface roughness is of no consequence and is effectively ruled out of this calculation.

The exchange current i_o can also be determined from the same measurements; from eqns 10 and 11

$$\frac{\eta_{a1}}{\eta_{a2}} = \frac{\ln (i_1/i_{oa})}{\ln (i_1/i_{oa})}$$

$$\text{i.e. } \left(\frac{i_1}{i_{oa}}\right) \eta_{a2} = \left(\frac{i_2}{i_{oa}}\right) \eta_{a1}$$

$$\text{i.e. } i_{oa}^{-\eta_{a2}} \; i_{ca}^{\eta_{a1}} = i_1^{-\eta_{a2}} \; i_2^{\eta_{a1}}$$

$$\text{i.e. } i_{oa} = \frac{i_2^{\eta_{a1}}}{i_1^{\eta_{a2}}}^{1/(\eta_{a1} - \eta_{a2})} \qquad (13)$$

To simplify the calculations involved above, and to enable calculation of the error introduced into these calculations in the measurements of current density and voltage, a computer program (Program II, see Appendix 8.3) was written to calculate α and i_o from measurements taken from photographs of the current calibration curve and polarised electrode potential waveform. The error calculations were made by repeating the main calculations twice; once each with all measurements at their limit, firstly so that a minimum estimate of α or i_o is obtained, secondly so that a maximum estimate of α or i_o is obtained. Table 1 shows the values of α and i_o so obtained for a number of replicate runs.

Table 1

α	Min. α	Max. α	i_{oa}	Min. i_{oa}	Max. i_{oa}	
.058	.057	.060	1.44×10^{-2}	1.08×10^{-2}	1.82×10^{-2}	
.027	.026	.028	3.60 "	3.28 "	3.95 "	All i_o in amp/cm^2.
.082	.078	.086	1.35 "	0.787 "	2.12 "	
.042	.039	.045	4.36 "	3.31 "	5.57 "	
.113	.109	.117	7.39×10^{-3}	6.41×10^{-3}	1.32 "	
.059	.057	.062	3.35×10^{-2}	2.85×10^{-2}	4.91 "	

Best estimate of α = 0.064 90% c. limits .018 and .110

Best estimate of i_o = 2.06×10^{-2} 90% c. limits 7.13×10^{-3} 5.93×10^{-2}

A section was also built into the program to calculate mean and 90% confidence limits from a number of similar runs. Fig. 11 shows the mean Tafel line obtained from successful runs (Table 1) in 1N.KCl + .00033M $AlCl_3$ pH 3.2 solution with the dotted lines showing the lines obtained from 90% confidence values of α and i_o.

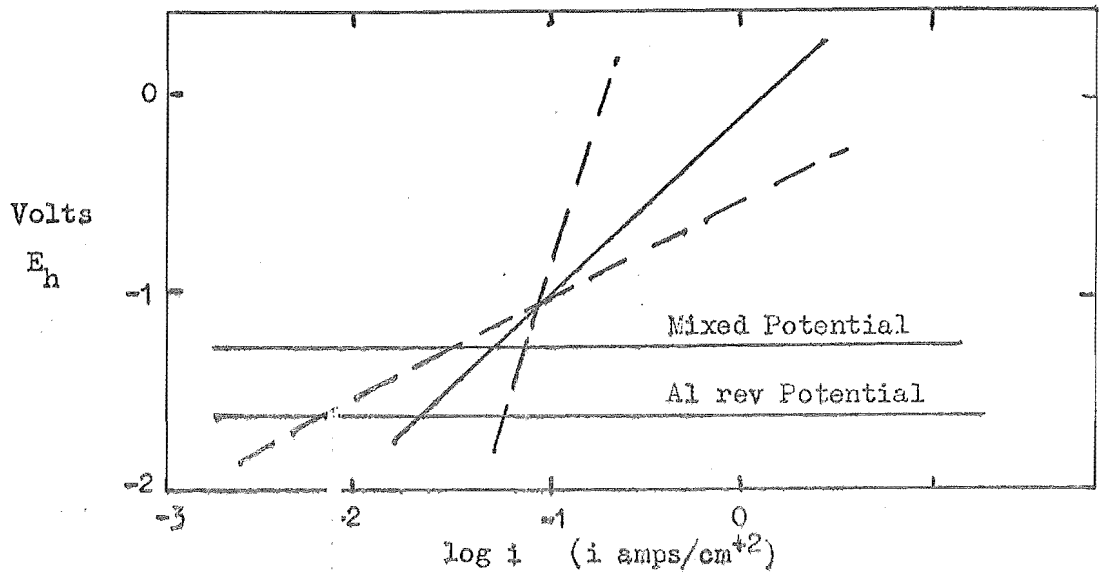

Fig. 11. Anodic Tafel line, α = .064, $i_o = 2.1 \times 10^{-2}$ amps/cm^{+2}
90% c. limits .018 to .110 i_o 5.93×10^{-2} 7.13×10^{-3}

The variation between runs is seen to be greater than that accountable to error in measurement. Also the measurements made in this way are even more scattered than might be expected from the variability of the electrode surface (e.g. work hardening) and it was realised that a further additional variation might be in IR drop in solution. This was significant because of the restricted current path (see geometry below) and the comparatively high current densities necessarily used in the experiments. The complex geometry of the electrode-solution-cutter (shown in Fig. 12) at the time of these potential measurements rules out any reasonable correction of IR drop

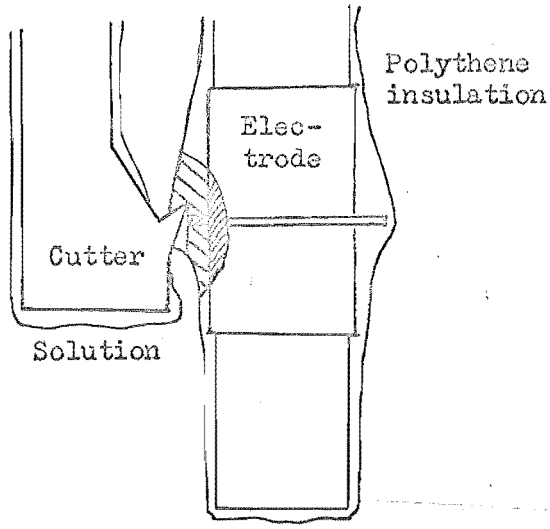

Fig. 12. Electrode-solution-cutter geometry just after cutting, showing restricted current path.

by calculation. Any such calculation is further complicated by the movement of the electrode throughout this period. It was thus reasoned that an experimental method should be developed to determine the solution IR drop at any time during the run and so correct for it in the calculations of α and i_o. The reader might think at this stage that such an IR drop would be easily observed as a sudden jump in potential on the change of current. This is, however, not possible in this case because

(a) the stray capacitances present with the IR drop, and

(b) the very high speed of the aluminium dissolution process provides similar time constants so that the fast rise due initially to the time constant stage of the capacitor-resistance, changes smoothly to the potential time waveform of the electrode process proper.

Fig. 13(a) shows diagrammatically the electrically important components in the cell at this time. Fig. 13(b) shows the voltage time response of each part (a) and (b) above and the combined response showing that a sudden IR drop is not observed. Hence another method had to be used.

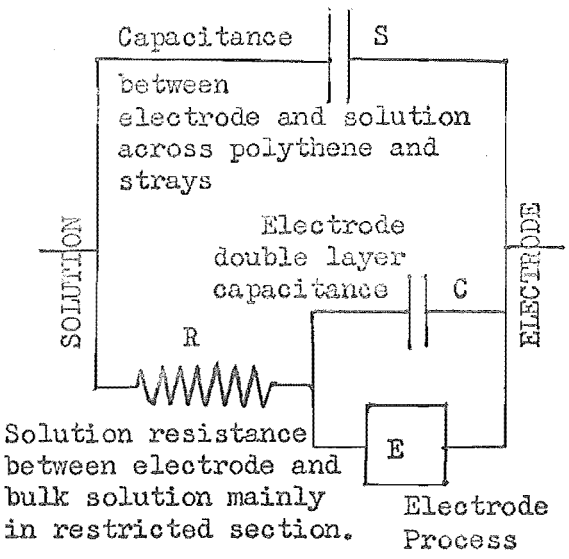

Fig. 13(a) Electrical components present in cell immediately after cutting.

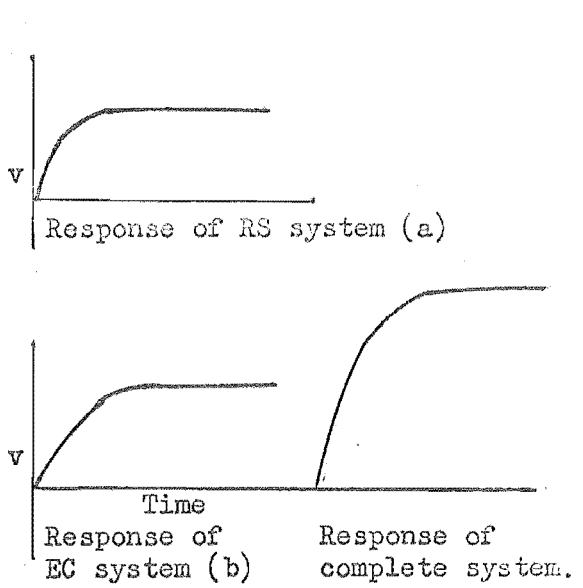

Fig. 13(b) Voltage time response of important components in cell showing how stray capacitance eliminates straight IR drop.

4.2.2 Turret Method or Three-level Square Wave Measurements

From eqn 9 introducing IR drop, one gets

$$U = \frac{RT}{\alpha_a F} \ln i/i_o + iR \qquad (14)$$

where it is desired to obtain α_a, i_o and R. U is apparent overvoltage. This suggested that if three equations could be obtained then the three unknowns, α_a, i_o and R, could be calculated. With this in mind, two pulse generators were connected together in such a way that a three-level (turret) pulse was obtained. Fig. 14 shows the current calibration photograph of such a pulse. Fig. 15 shows the potential time trace produced by a typical anodically-loaded aluminium electrode.

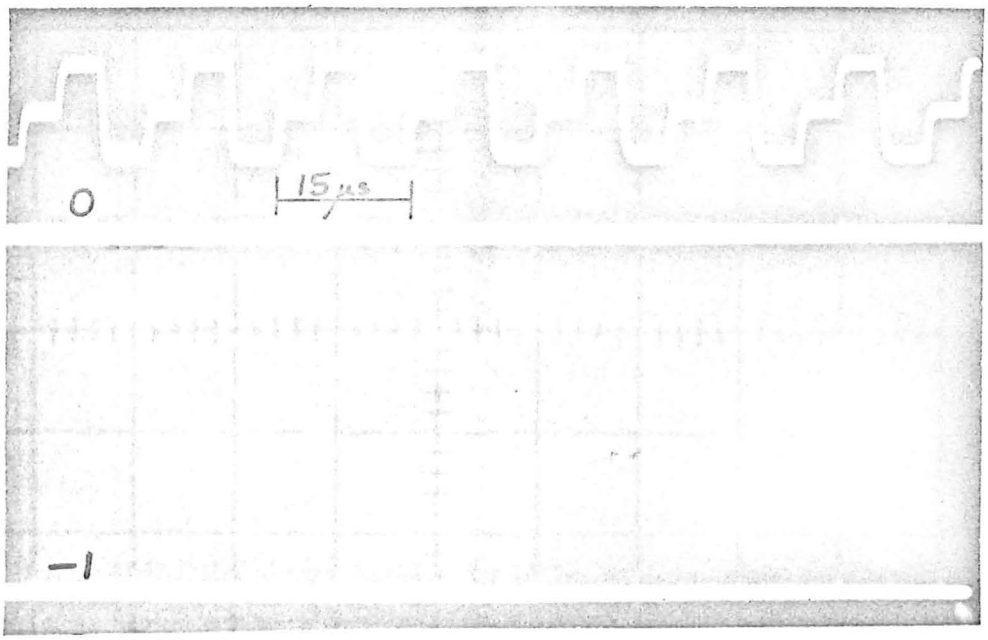

Fig. 14. Anodic turret or three-level current measurement trace. 0 is zero volts (i.e. shorted condition); -1, one Weston cell negative of 0.

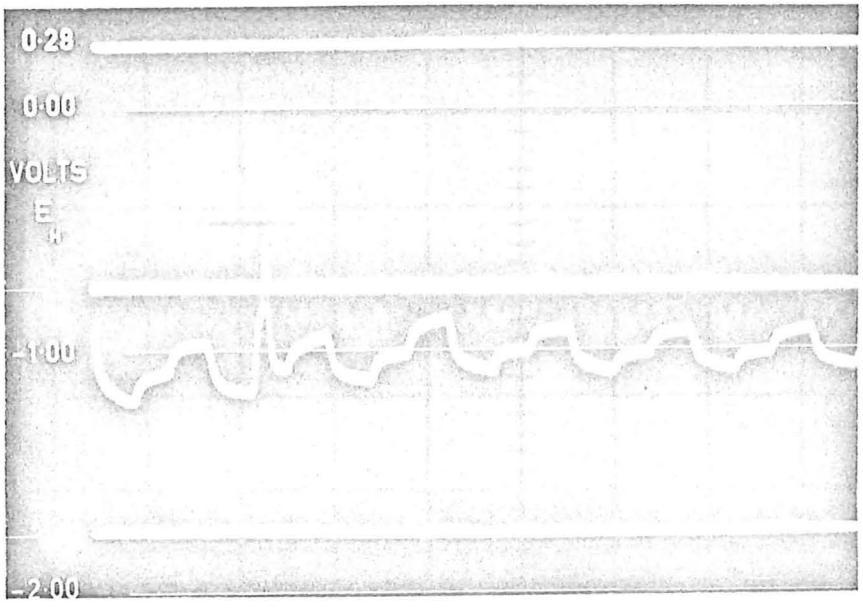

Fig. 15. Trace of electrode potential anodically polarised by turret wave current loading.

Eqn 14 thus gives for each level

$$\begin{aligned} U_1 &= \frac{RT}{\alpha_a F} \ln i_1/i_{oa} + i_1 R \\ U_2 &= \frac{RT}{\alpha_a F} \ln i_2/i_{oa} + i_2 R \\ U_3 &= \frac{RT}{\alpha_b F} \ln i_3/i_{oa} + i_3 R \end{aligned} \qquad (15)$$

by substituting $y_i = \ln i_i$ $\quad k = \ln i_{oa}$ $\quad b = \frac{RT}{\alpha F}$

one gets

$$\begin{aligned} U_1 &= by_1 - bk + Re^{y_1} \\ U_2 &= by_2 - bk + Re^{y_2} \\ U_3 &= by_3 - bk + Re^{y_3} \end{aligned} \qquad (16)$$

from eqn 16 eliminating k

$$\begin{aligned} U_1 - U_2 &= b(y_1 - y_2) + R(e^{y_1} - e^{y_2}) \\ U_1 - U_3 &= b(y_1 - y_3) + R(e^{y_1} - e^{y_3}) \end{aligned} \qquad (17)$$

eliminating b from eqns 17

$$\frac{y_1 - y_2}{y_1 - y_3} = \frac{U_1 - U_2 + R(e^{y_2} - e^{y_1})}{U_1 - U_3 + R(e^{y_3} - e^{y_1})}$$

from which

$$R(y_1 - y_3)(e^{y_2} - e^{y_1}) + R(y_2 - y_1)(e^{y_3} - e^{y_1}) = (y_1 - y_2)(U_1 - U_3) + (y_3 - y_1)(U_1 - U_2)$$

and thus

$$R = \frac{\ln i_1/i_2 \,(U_1 - U_3) - \ln i_1/i_3 \,(U_1 - U_2)}{\ln i_1/i_2 \,(i_1 - i_3) - \ln i_1/i_3 \,(i_1 - i_2)} \qquad (18)$$

Similarly, by eliminating R from eqns 17, b can be obtained, viz:

$$b = \frac{(i_1-i_3)(U_1-U_2) - (i_2-i_3)(U_1-U_3)}{\ln i_1/i_2\,(i_1-i_3) - \ln i_1/i_3\,(i_1-i_2)} \qquad (19)$$

thus giving α_a from $\alpha_a = \frac{RT}{Fb}$

Substituting b into R into say the first eqn 16 gives

$$k = \frac{\ln i_1 - U_1 + i_1 R}{b}$$

from whence $i_o = e^k$.

It very quickly becomes evident on substituting actual values from a run into these expressions for R, α and i_o that the eqns 15 are not well conditioned for the range of i obtainable experimentally. In fact accuracy not remotely attainable with present equipment would have to be obtained to determine the parameters α_a, i_o and R in this way.

An example of the ill condition present is shown in Table 2 below where the values of current density and voltage are shown in line 1 as measured, together with α_a and R calculated from them. Line 2 is identical except for say a remeasurement of U_2 which is 8 mV larger. The α_a and R are then calculated from these values.

Table 2

	i_1 amp/cm^2	i_2 amp/cm^2	i_3 amp/cm^2	U_1 volts	U_2 volts	U_3 volts	α_a Calc. from eqns 17 and 18	RΩcm^2
1.	.0717	.1238	.1780	.708	.881	1.056	1.077	3.06
2.	"	"	"	"	.889	"	0.239	2.38

Fig. 16 demonstrates this point even more markedly where the points in Table 2 are plotted; line A being the Tafel line corrected for IR

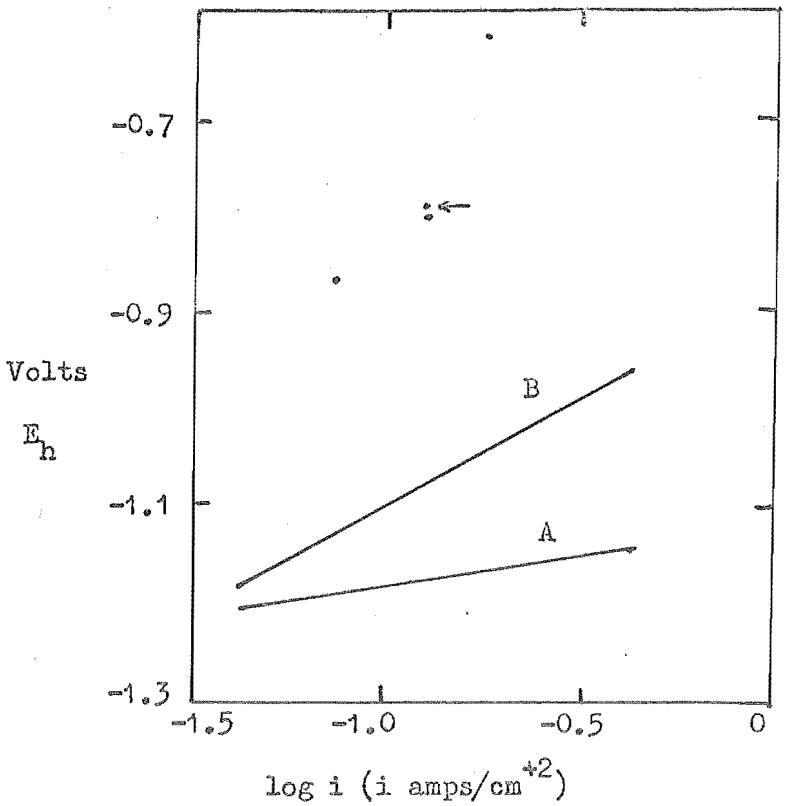

Fig. 16. Anodic turret example from Table 2 results showing ill condition. E_h = U - 1.67v.

drop obtained from line 1, table 2. Line B is the Tafel line corrected for IR drop using the remeasured U_2 (arrowed point), from line 2.

When it is realised that errors will be present in all the other variables as well, it can be seen that the values so obtained are almost meaningless. Thus another method had to be found for these determinations.

4.2.3 No-Load Curve Analysis

It had been noticed by the author in obtaining the theoretical curves presented in section 2.1, that the shape of the potential time curve from the time of cutting until the peak potential was reached depended very strongly on the parameters α_a, i_{oa} and C. This suggested naturally that the parameters should be able to be obtained from an analysis of this curve. For the anodic process alone with no polarisation, eqn 6 (p.9) became

$$C\frac{d\eta_a}{dt} = i_{oa}\left(e^{-\frac{\beta_a z F \eta_a}{RT}} - e^{\frac{(1-\beta_a) z F \eta_a}{RT}}\right)$$

η_a is positive and when greater than 50 mv $e^{-\frac{\beta_a zF}{RT}}$ is negligible.

Thus

$$C\frac{d\eta_a}{dt} = -i_{oa}\, e^{\frac{\alpha_a F \eta_a}{RT}} \qquad \text{where } \alpha_a = (1-\beta_a)z$$

removing subscripts from η and α and integrating

$$t = -\frac{C}{i_{oa}} \int_{\eta_o}^{\eta} \frac{d\eta}{e^{\frac{\alpha F \eta}{RT}}} \qquad \text{where } \eta = \eta_o \text{ at } t = 0.$$

$$t = \frac{C\,RT}{i_{oa}\,\alpha F}\left(e^{-\frac{\alpha F \eta}{RT}} - e^{-\frac{\alpha F \eta_o}{RT}}\right)$$

It can easily be seen from the above equation that C and i_{oa} are mutually dependent in terms of time and overvoltage. Thus only α and the ratio of C to i_{oa} could be determined from the analysis of an unpolarised electrode potential curve. As a simple analytical regression solution to this equation was not known, a "hill climbing" procedure was used to determine α and the ratio C to i_{oa}. This involved altering α from a given estimated value by small increments until the sum of squares

of the deviations of the calculated times for given voltages from the observed times for those voltages was a minimum. i_{oa} was then altered (C was held constant) by small increments until i_{oa} was also an optimum according to this same criterion. α was then optimised again and subsequently i_{oa} and so on until no further change in α or i_{oa} gave any improvement in fit. To accomplish this economically, the above procedure was incorporated in a computer program (Program III, Appendix 8.4).

Fig. 17 shows a photograph of a typical unpolarised electrode potential trace from about a microsecond after cutting has started. At a scan speed of the order used in these runs it is necessary to trigger the trace on the potential fall itself, and to avoid spurious triggering it was found by experience that a trigger starting level of about 0.5 volt had to be used. Thus, in spite of using the built-in delay line in the Tektronix oscilloscope, the potential is not seen from the initiation of cutting.

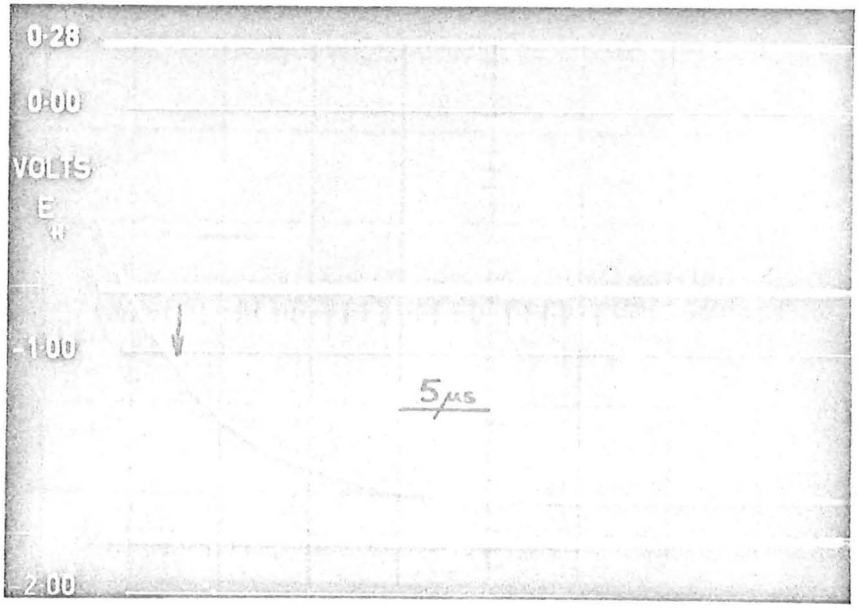

Fig. 17. Unpolarised electrode potential trace showing initial fall detail. Arrow shows point at which cutting was completed.

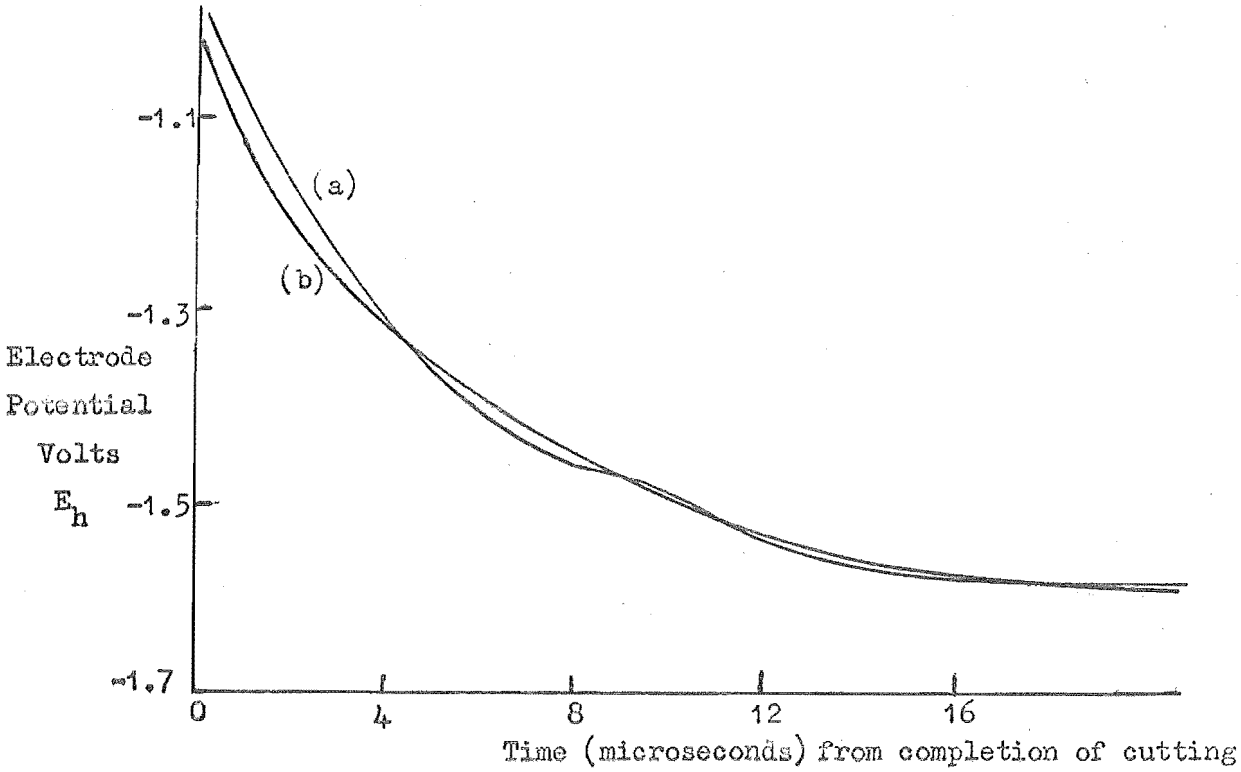

Fig. 18. Comparison of actual curve with best fit curve fitted by Program III. (a) actual curve, (b) fitted curve. Only points from the actual curve after cutting was completed were used in the fitting. Parameters obtained were $\alpha = 0.104$, $C/i_{oa} = 7.0 \times 10^{-5}$ F/amp

Fig. 18 shows this same curve together with the theoretical curve fitted by Program III.

Calculation of α and the ratio C/i_{oa} using only that part of the curve where cutting had been completed, was done for the two runs where this was possible (cutting time was short enough), and the average values found were $\alpha = 0.1$, $C/i_{oa} = 6.5 \times 10^{-5}$ F/amp. It is found, however, that cutting, i.e. creation of new electrode surface, does not seem to affect greatly the above parameters obtained by this method as is shown by comparing (see Table 3 below) the values above with those obtained using other runs in which cutting was occurring during the whole or part of the potential rise used for the measurement.

Table 3

	α	C/i_{oa} (F/amp)	
1	.104	7.0×10^{-5}	Measurements taken from curve after cutting completed
2	.095	6.0 "	
3	.093	4.9 "	Cutting occurring over full measurement
4	.102	5.1 "	" " " half "
5	.081	6.7 "	" " " half "
6	.094	7.6 "	" " " full "
7	.104	4.8 "	" " " quarter "
8	.096	3.4 "	" " " full "
Mean of 3-8	.095	5.4 "	
Overall mean	.096	5.7 "	

Another observation which shows that cutting apparently has little effect is the fact that, in general, no definite discontinuity on the curve can be found where cutting has been completed. If the creation of electrode surface as occurs during cutting did affect the potential time curve obtained, then it would be expected that on cessation of cutting a discontinuity in the potential time curve would be obtained.

This apparent lack of effect of cutting on the kinetic parameters is surprising and difficult to interpret. It suggests that the electrode-solution capacitance, whether due to the conventional electrical double layer or not, does not change its capacity with time, at least in the potential region where cutting generally finishes. This may mean that the zero charge potential for aluminium in this situation is about -1.6v or that the establishment of the usual electrical double layer is a slow process compared with that usually quoted[38].

The first of these possibilities could be tested if a method could be found for exposing a fresh metal surface to the electrolyte in, say,

a fraction of a microsecond. In this case a discontinuity at cessation of cutting would appear in the potential time trace obtained. The second explanation would show no such discontinuity and is supported slightly by the double-layer capacities measured at this time (see table 4 below) which are unusually low; nearly an order lower than the double-layer capacities measured a millisecond later in this potential region (section 4.4).

Further slight support for the second possibility is offered by earlier measurements on those runs in which cutting was completed before measurements were made (i.e. 1 and 2, Table 3). If these earlier points on the curve before cutting was complete were used in the regression analysis (Program III) then lower values of α and C/i_{oa} were obtained (e.g. cf 1, Table 3, with $\alpha = .093$ and $C/i_o = 6.5 \times 10^{-5}$ F/amp).

If now the α obtained above is used in conjunction with the turret or ordinary square wave polarised runs (sections 3.2.1 and 3.2.2) and the difference in α between these is due to solution IR drop alone, then this can be determined using eqn 14 and hence i_{oa} can be obtained. If this is then used with the value of C/i_{oa} ratio found also from the unpolarised runs, a value for the double-layer capacity for the aluminium electrode at this time is obtained. (The electrical double-layer capacity could not be obtained from the initial slope of the potential jump in the anodic square wave measurements for the same reason that the solution IR drop could not be simply obtained (see section 4.2.1), viz. because of the capacitance of the insulated electrode with respect to the solution together with the stray circuitry capacitances in parallel with this. Thus the initial slope if used for a capacitance determination would give the insulated electrode plus stray capacitance and not the double-layer capacity. This was, in fact, observed.)

Values of i_{oa} and C determined in this way are tabulated below (Table 4).

Table 4

orig. α	orig. i_{oa} amps/cm^2	i_{oa} (without IR drop) amps/cm^2	C μF/cm^2
.058	1.44×10^{-2}	1.7×10^{-2}	1.10
.027	3.60×10^{-2}	2.0×10^{-2}	1.30
.082	1.35×10^{-2}	1.3×10^{-2}	0.85
.042	4.36×10^{-2}	3.6×10^{-2}	2.34

4.3 Cathodic Square Wave Measurements in Chloride Solutions

All cathodically-polarised square wave potential measurements were made within the first five milliseconds after cutting. This time was sufficient to allow the electrode to clear the cutter, allow the hydrogen discharge process to become established and yet short enough so that concentration polarisation would not affect the measurements made[8].

4.3.1

A solution of 1N.KCl pH 3.2 was used throughout (cf. section 3.2.1, no Al ion) so that the only feasible cathodic process was the discharge of hydrogen as discussed in section 1.2.

A typical square wave current, cathodically-polarised electrode potential trace is shown in Fig. 19.

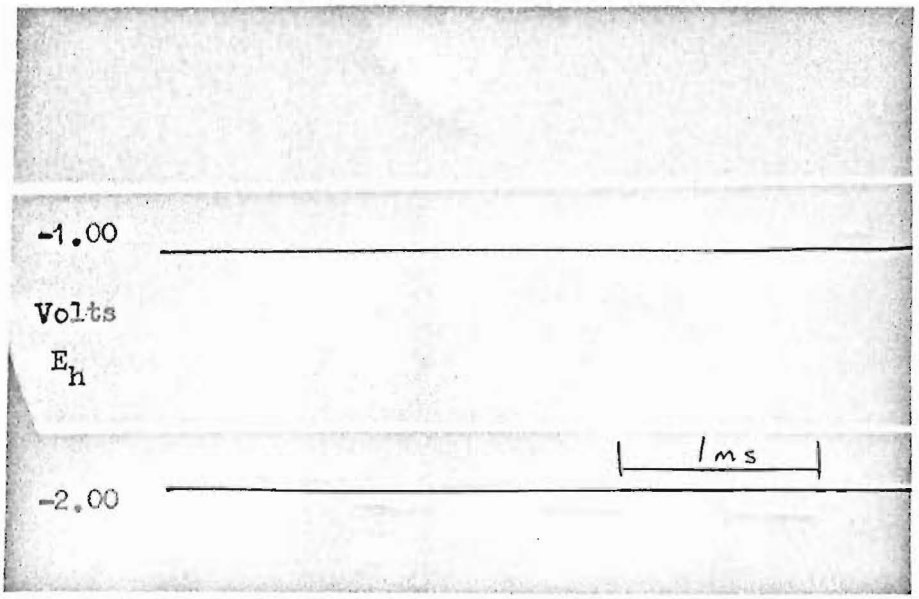

Fig. 19. Typical square wave cathodically polarised electrode potential trace in 1 N.KCl pH 3.2.

The conditions with regard to current density and potential for the potential flats are similar to those obtained in section 3.2.1 except that the process is purely cathodic. Thus eqn 6 reverts to eqn 2 at steady state and when only the cathodic process occurs on the electrode and so equations analogous to 10, 11, 12, 13 are obtained with i_{oc}, α_c, n in place of i_{oa}, α_a and z respectively.

Program II (discussed in 3.2.1) was therefore used to calculate values of α and i_o and the measurement errors in these. Another small section of Program II was used to make a correction for the IR drop which affected the parameters obtained and was most significant in the solution closest to the electrode. For this correction the resistance of a segment of a sphere (radius 0.2 cm) whose angle was equal to the cutter angle was used. The current path in this segment for the purpose of the calculation was considered as purely radial and the cut

area spherical with radius such that the electrode area in this model was equal to the apparent electrode area as measured under the microscope.

As with the anodic results, the mean values and 90% confidence values corrected in some measure for IR drop as outlined above, were determined (see Table 5) and the Tafel lines resulting are plotted in Fig. 20.

Table 5

α	Min. α	Max. α	i_{oc}	Min. i_{oc}	Max. i_{oc}
.235	.212	.262	1.2×10^{-8}	2.7×10^{-10}	1.8×10^{-7}
.196	.177	.222	3.3×10^{-7}	2.2×10^{-8}	2.4×10^{-6}
.233	.201	.281	9.0×10^{-9}	4.5×10^{-11}	2.9×10^{-7}
.257	.218	.317	1.2×10^{-9}	3.2×10^{-12}	5.2×10^{-8}
.239	.228	.252	3.7×10^{-8}	3.1×10^{-9}	2.7×10^{-7}
.195	.183	.210	9.2×10^{-8}	1.6×10^{-8}	4.0×10^{-7}

In this case the deviation between runs could well be accounted for by the error arising in measurement (see Table 5) so that the most probable values for i_o and α are 2.3×10^{-8} and 0.225 respectively with 90% confidence values of 1.2×10^{-9} and 4.4×10^{-7} for i_o, and .262 and .188 for α for hydrogen evolution on aluminium in 1N.KCl pH 3.2.

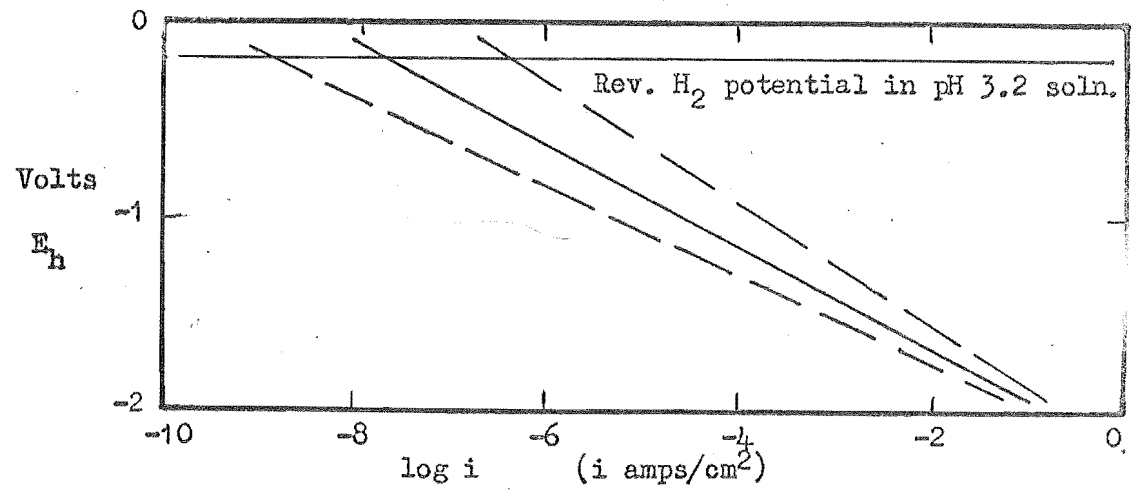

Fig. 20. Cathodic Tafel line $\alpha = 0.225$ and $i_o = 2.3\times10^{-8}$
90% confidence limits α, .188 and .262
i_o 4.7×10^{-4} and 1.2×10^{-9}. Note extrapolation.
All measurements were made at about -2v.

4.4 Unpolarised Potential Time Trace Simulation

The potential time trace obtained using the best estimates of anodic and cathodic parameters and assuming that the electrode function changes fairly rapidly (exponentially with T = 0.2 ms) from anodic to cathodic (starting to do so after a 20 μs delay) was calculated and is shown as curve (b) in Fig. 21. Curve (a) is a typical no-load curve obtained experimentally (curve (a), Fig. 3). The anodic parameters (section 4.2.3) were $\alpha_a = 0.10$, $i_{oa} = 2.15 \times 10^{-2}$ amp/cm^2 and C = 1.4 μF/cm^2. The best cathodic parameters (section 4.3.1) were $\alpha_c = 0.225$, $i_{oc} = 2.3 \times 10^{-8}$ amps/cm^2. C used for that part of the curve after the area changeover starts, was that measured from square wave polarisations in the mixed potential region (viz. 7.6 μF/cm^2). The two remaining curves (c) and (d) were obtained using the 90% confidence values for the cathodic parameters.

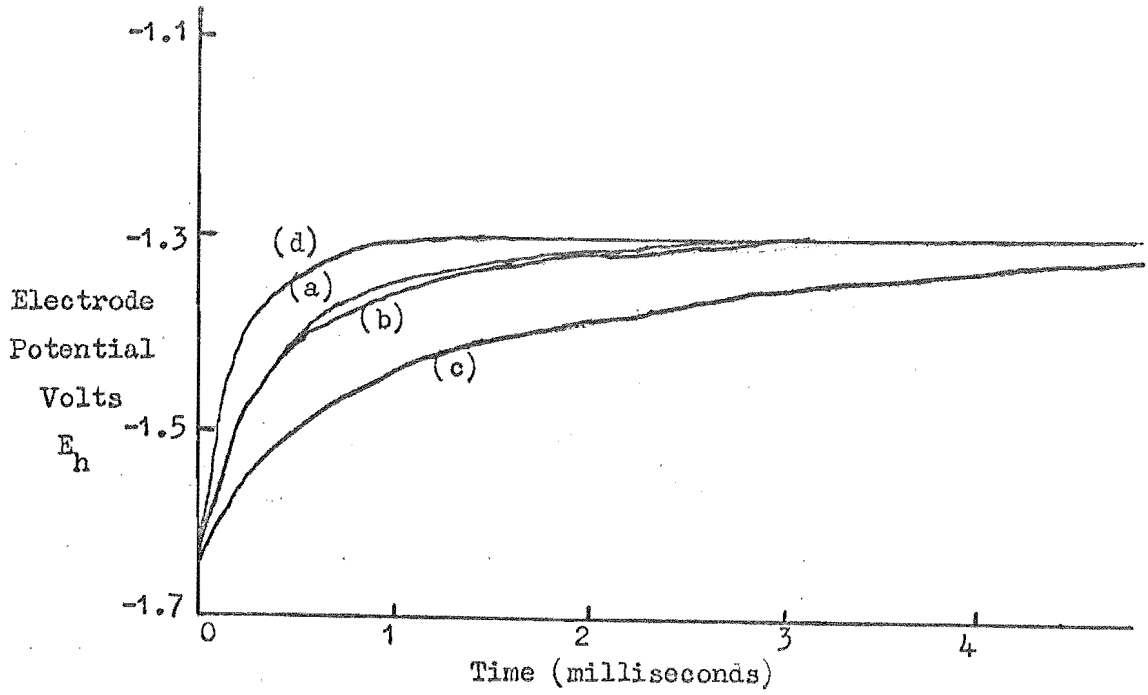

Fig. 21. Predicted no-load curves compared with experimental curve. (a) Experimental curve. (b) Predicted curve using best estimates of anodic and cathodic parameters with 20 μ sec delay before area changeover starts. (c) and (d) as for (b) except using 90% confidence values of cathodic parameters.

Curve (a) in Fig. 22 is the same curve as (a) in Fig. 21. The remaining curves show the results of (b) area ratio changing more slowly (viz. T = 2 ms) still starting to do so after 20 μs, (c) starting the change in area ratio from time zero with T = 0.2 ms and not from 20 μsec after changing, (d) starting the change in area ratio from time zero with T = 2 ms. Whether the area ratio changes with T = 0.2 ms after 20 μsec delay or instantaneously by a step after this same delay makes no significant difference to the resulting curve. However, if the peak is examined in closer detail, i.e. by expanding the time scale, then the instantaneous changeover is seen to cause a break in the computed curve whereas the more gradual changeover gives a smooth curve. As no break was observed in the experimentally obtained traces this suggests that the changeover was smooth and not discontinuous.

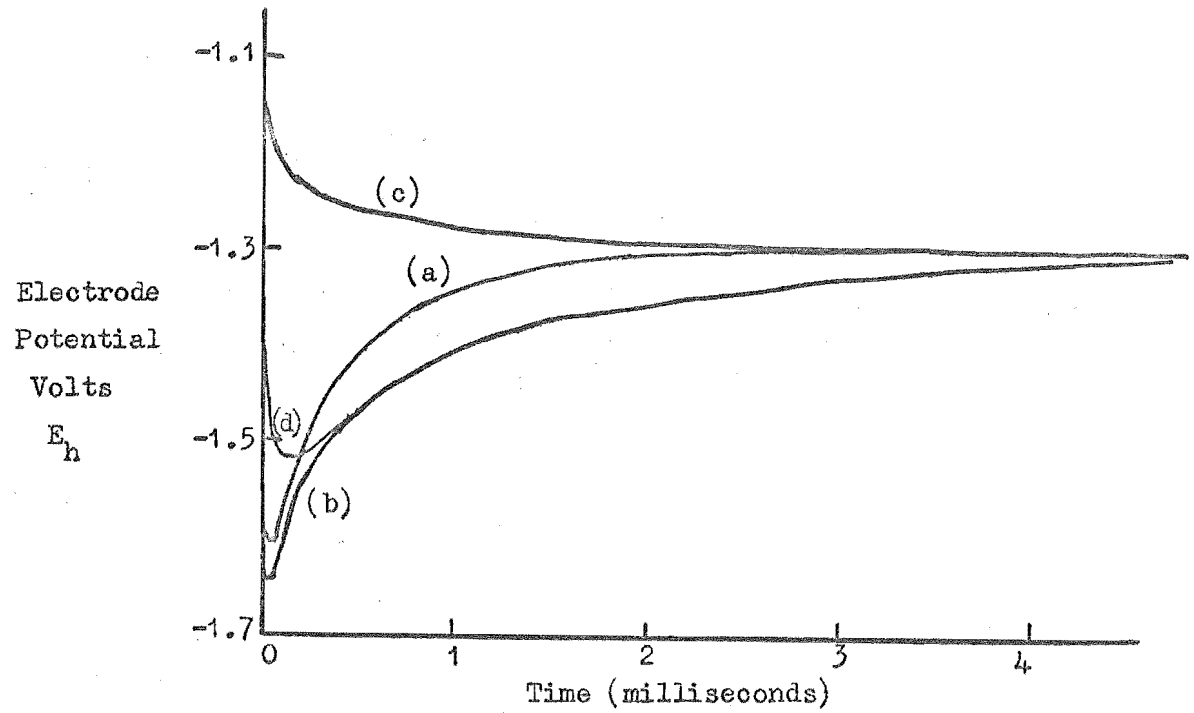

Fig. 22. Predicted no-load curves compared with
(a) Experimental curve, (b) Predicted curve slower area ratio changeover (T.C. = 2ms) still 20 μsec. delay. (c) and (d) no delay
(c) T.C. of changeover 0.2 msec
(d) T.C. as for (b), i.e. 2 msec.

It is entirely feasible and indeed probable that the previously assumed delay before changeover commences is not a pure delay as postulated earlier but that the area ratio changes over as a second or higher order exponential type curve as shown in Fig. 23. The accuracy obtainable at present does not permit resolution of this point and no attempt has been made to determine coefficients for such a function as suggested above. Providing the area ratio is close to zero for some 20 μsecs or so after cutting and then rapidly increases to its maximum value, the experimentally observed potential time traces are explained. It would be comparatively easy to incorporate a more complicated changeover function into Program I when it became justified.

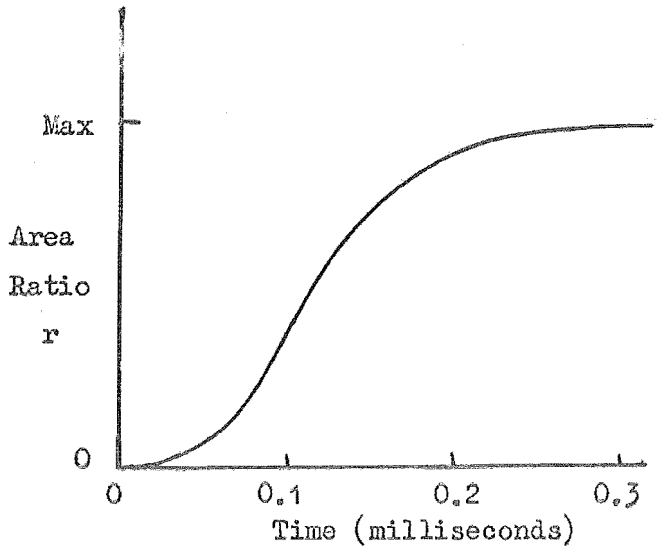

Fig. 23. Possible area ratio changeover.

The reasons for this delay in initiation of area changeover are difficult to surmise. The phenomenon of the peak potential is not confined to aluminium but certainly occurs with magnesium and titanium and presumably with many other metals of high electronegativity so that the explanation of area function changeover would apply on these metals as well. A no-load trace for magnesium is shown in Fig. 24 below and no-load traces for titanium can be seen in Wakelin's work[39].

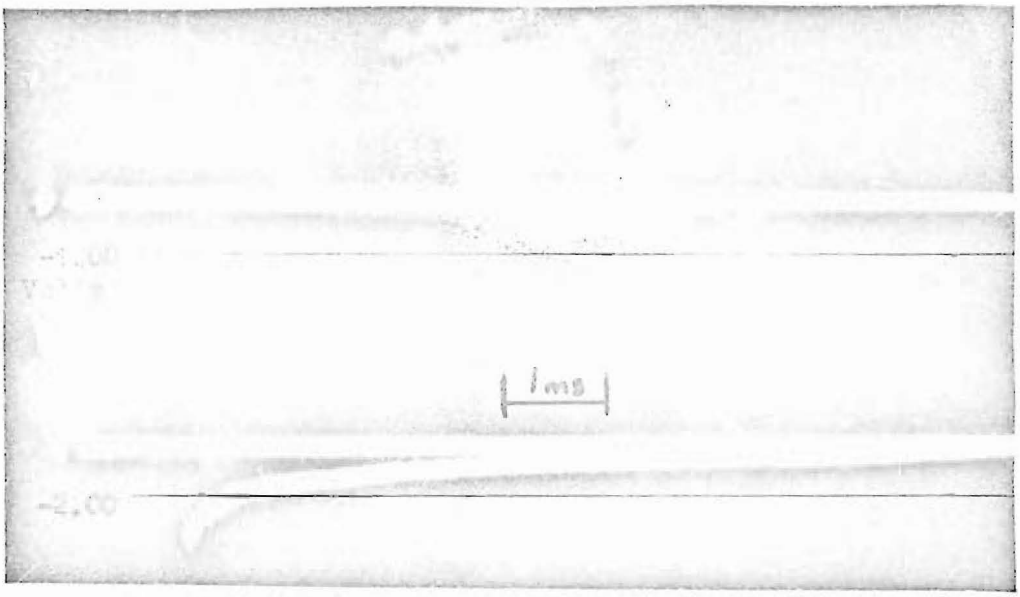

Fig. 24. No-load electrode potential trace for magnesium in 1 N.KCl pH 3.2.

It might be thought that a possible cause of this delay could be the necessity for accumulation of adsorbed hydrogen atoms on the metal surface, the hydrogen atoms so adsorbed inhibiting the anodic dissolution process and concurrently aiding the hydrogen discharge process possibly by the Electrochemical Mechanism of Bockris and Potter[41], viz:

$$H_3O^+ + e \longrightarrow MH + H_2O$$

$$H_3O^+ + MH + e \longrightarrow H_2 + H_2O$$

where M is a metal atom on the electrode surface.

This possibility is easily ruled out by a simple calculation which shows that less than 2% of a monolayer of hydrogen atoms could be deposited in 200μsec at which time it has been found that the electrode surface should be 99% cathodic. Another point which counts strongly against the above argument is that if the cathodic process producing this adsorbed hydrogen were occurring at anywhere near the rate needed to get even a 2% cover, then no peak would be obtained.

A reasonable explanation for this could involve the orientation of the adsorbed water molecules at the surface of the metal. At relatively positive potentials, molecular water is presumably adsorbed with the negative end of the dipole towards the metal surface (see Fig. 25(a)); at relatively negative potentials with the positive end towards the metal surface (see Fig. 25(b)). Bockris et al[40] show that considerable doubt exists concerning the potential at which reversal of the dipole occurs even on mercury, the most commonly studied metal in this field. No information is available for aluminium.

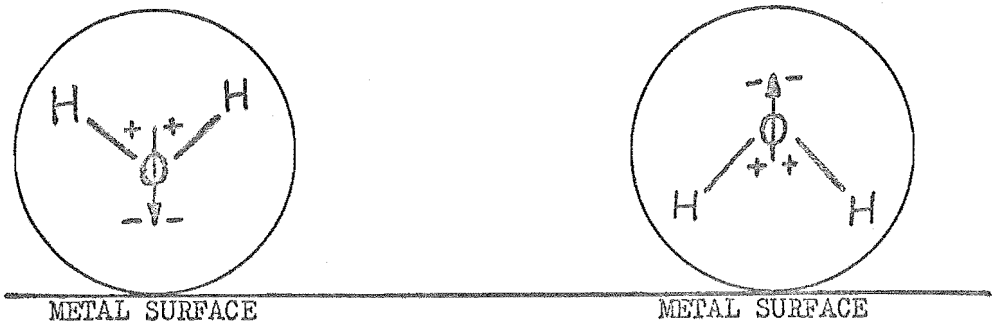

Fig. 25(a) Water Molecule Adsorbed oxygen end to metal.

Fig. 25(b) Water Molecule Adsorbed hydrogen end to metal.

If it is now assumed that hydrogen discharge cannot effectively occur with the oxygen end of the water molecule adsorbed and that the reversal or reorientation process is a process taking longer than, say, 20 μsec, then the observations made are partly explained. Thus, if water is adsorbed very rapidly oxygen end to the metal in the potential range in which most of the cutting occurs and then as the potential becomes more negative reorientation of the adsorbed water molecule occurs, the hydrogen discharge process can occur. It would also seem necessary that the water molecules adsorbed hydrogen end to metal, besides being necessary for the hydrogen ion discharge process,

somehow stifle the anodic dissolution process. This argument is supported slightly by the fact that there is no observable delay in the initiation of the hydrogen ion discharge process when the electrode is cathodically loaded, i.e. maintained much more negative before and during cutting (see Fig. 26).

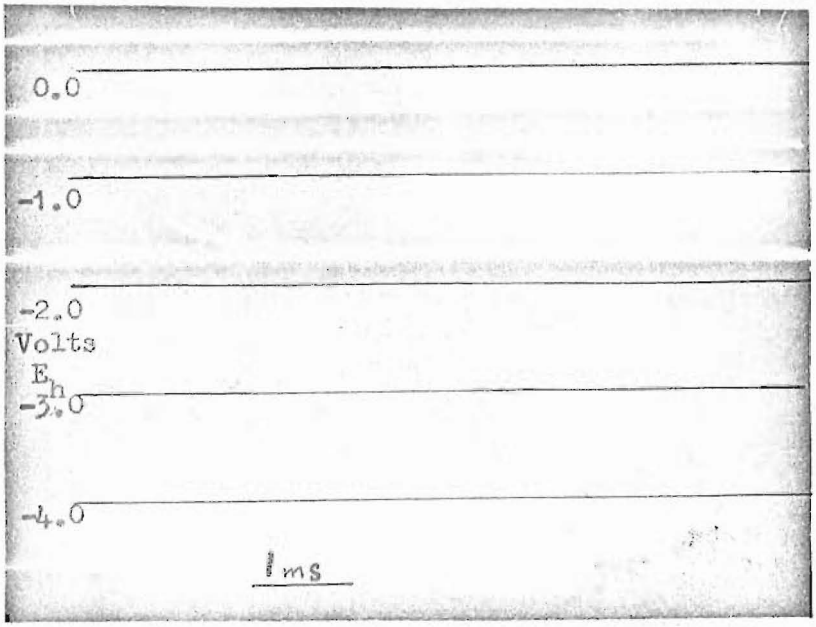

Fig. 26. Cathodically polarised electrode potential trace on coarse volt scale showing no apparent delay in initiation of cathodic process.

Another possible explanation of the delay is that the adsorption of water no matter the orientation is a relatively slow process (somewhat greater than 20 μ sec, say) and that this adsorption both stifles or inhibits the anodic dissolution process and is necessary for the hydrogen discharge process to occur at all; the water or other molecule being an intermediary in the electron transfer process.

Further support for the adsorption of water theories is given by the no-load behaviour of the aluminium electrode in 98% methanol solution saturated with KCl (see Fig. 27). In this case the

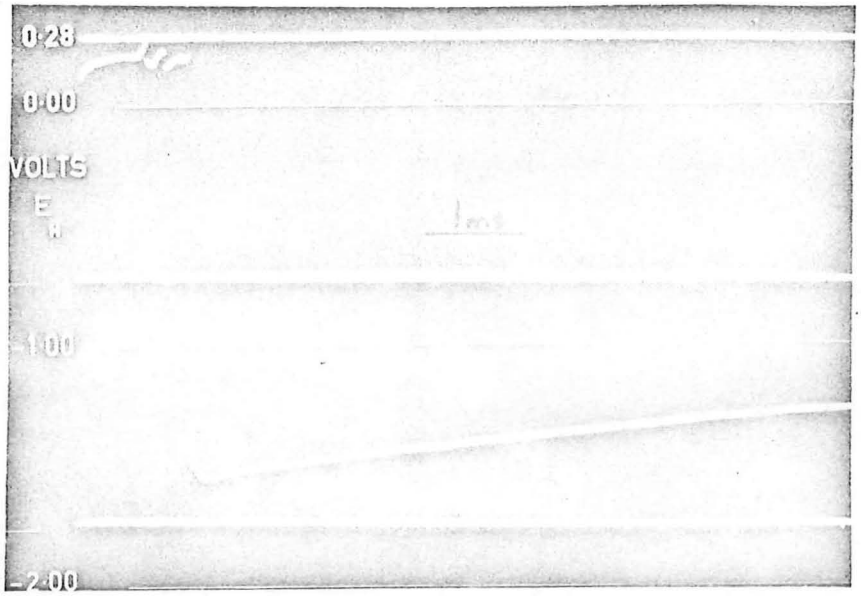

Fig. 27. No-load electrode potential trace in methanolic solution.

cathodic parameters in methanol solutions, although not very reproducible, suggest that the decay to the mixed potential should be faster than in 1N.KCl aqueous solution as is observed in sulphate solutions (section 4.5.2). Lower overvoltages in methanolic solutions have been reported[42] previously for other metals. The fact that the decay to the mixed potential is much slower could be explained by the adsorbed methanol molecules reorientating at a much slower rate than water molecules, which seems reasonable in view of the larger size of the methanol molecule. This would account for the slower decay to the mixed potential in spite of the probably more favourable discharge parameters.

4.5 Measurements with other Electrolytes and Electrode Materials

In an attempt to determine which, if any, of the foregoing results were specific to chloride ion or pH in solution, a number of runs were done in sulphate solutions and in solutions of different pH. A few runs were made in chloride solutions using aluminium of a different purity. No difference was observed among runs using aluminium of different grades, at least in the range of three purities available here (see section 3.4). This indicates that the impurities present are certainly not present as pure components for if iron, say, were present as normal metallic iron at the minimum concentration specified, for instance, then the current carried by the iron at the usual potentials measured (assuming normal overvoltage parameters for iron) would be about 1000 times that carried by the aluminium (i.e. that measured) at the same potential.

4.5.1 Anodic Measurements in Sulphate and other Chloride Solutions

Square wave runs made in ~~the~~ 1N.K_2SO_4 + .00033 N.$Al_2(SO_4)_3$ solutions of pH 2, 3, 4 and 1N.KCl + .00033 N.$AlCl_3$ solutions of pH 2 and 4 within the first 50 μsec of cutting were not significantly different from each other or from the similar runs in chloride solution pH 3.2 (section 4.2.1) within the accuracy of the experiments. This does not in fact mean that there was no difference, for the variability was equally as great as in section 4.2.1, but it would seem to indicate that the anodic reaction is independent of the anion present at least for chloride and sulphate in the potential region and in the times covered in these runs. The other possibility that the anodic reaction was equally dependent on chloride and sulphate ion seems unlikely.

That the anodic reaction appears independent of pH in this range is expected. Thus the observations so far made in this respect suggest that the anodic reaction probably only involves aluminium ions, viz:

$$Al \longrightarrow Al^{+++} + 3e$$

or $$Al \longrightarrow Al^{+} + e$$

$$Al^{+} \longrightarrow Al^{++} + 2e$$

at least in the time and potential region covered by these runs.

4.5.2 Cathodic Measurements in Sulphate Solution

Square wave runs were made in 1 N.K_2SO_4 pH 3.2 solution in a manner identical to those made in 1 N.KCl (section 4.3.1) with the surprising result that i_{oc} appears to be significantly larger and α significantly smaller than the comparable results in chloride even when IR drop corrections are made using the slightly higher resistivity of the sulphate solution. These results are:

best estimate $i_o = 7.9 \times 10^{-6}$ amps/cm^2 . $\alpha = 0.131$.

90% confidence limits 2×10^{-6} and 3×10^{-5} for i_o, 0.175 and .088 for α.

This means that even though the current density is less in sulphate than in chloride solutions in -2.0 volt region, the current required by the cathodic process at the mixed potential is higher in the case of sulphate than chloride, assuming of course straight Tafel line behaviour to the mixed potential region. Because of this, one would expect the decay to the mixed potential for an unloaded trace to be much faster in sulphate than in chloride solution. This is, in fact, observed. Fig. 28 shows a typical unloaded electrode potential trace in sulphate (b), together with the theoretical trace obtained using the above parameters

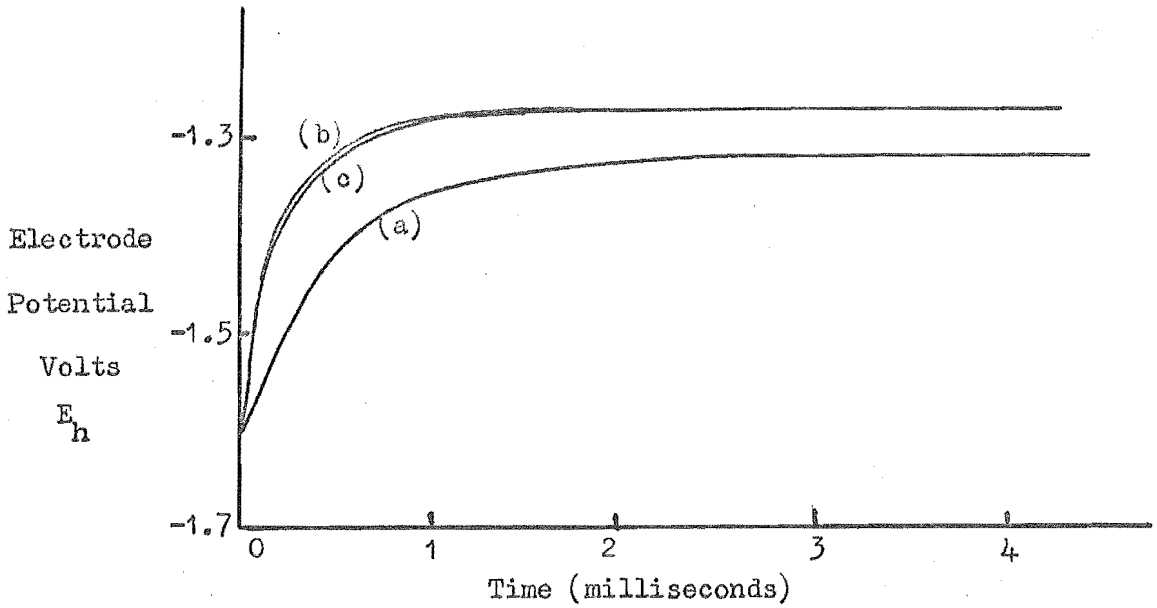

Fig. 28. Comparison of potential curves.
(a) actual trace in chloride solution ((a) from Fig. 21)
(b) actual trace in sulphate solution
(c) predicted trace in sulphate solution: all pH 3.2

(c), and an unloaded potential trace obtained in chloride (a) as in Fig. 21.

It was difficult at first sight to see why hydrogen ion should be more easily discharged (shown by the larger i_o) from sulphate solutions than chloride solutions of the same pH, at least at potentials more positive than ca. -1.7, as the only difference between them was the anion. This increase in i_o was possibly due to the difference in the structure of the electrical double layer as it seems unlikely that either anion would enter directly into the hydrogen discharge reaction. The most likely change in double layer structure is specific adsorption and, as has been observed previously, this may either decrease[31,32] or increase[33,34] the rate of electrode reactions.

It is well known from Grahame's work[35] that chloride ion is specifically adsorbed on mercury whereas sulphate is not. Bockris[36] has evidence that chloride ion is adsorbed qualitatively in the same way on Pt, Au, Cu, Ni and Fe.

It would seem unlikely at first sight that chloride ion would be specifically adsorbed at potentials as negative as these for as the electrode becomes more negative it would tend to repel anions and presumably desorb anions already adsorbed. Watson[28] has slight evidence that this might occur when he obtains hydrogen discharge parameters on aluminium in 1 N.KCl at very much longer times than those used in the present work and these are remarkably close to those obtained in sulphate solutions by the author.

Kolotyrkin[37] has definite evidence for specific halide ion adsorption decreasing the rate of the hydrogen discharge process on lead, cadmium, and thallium. He also shows that specific adsorption of these anions on these metals was occurring even at potentials as negative as -1.0v. It would thus seem likely that chloride ion was being specifically adsorbed on aluminium and also hindering the hydrogen discharge on this metal as suggested by the values of i_o determined (section 4.3.1, 4.5.2). This seems very much more probable than adsorption of sulphate aiding this reaction.

The change in α with anion suggests that a different step is exerting more control in this discharge reaction, most probably due again to the effect of specifically adsorbed chloride ion on the charge transfer process across the double layer.

4.5.3 Cathodic Measurements in pH 2.0 Solutions

Square wave runs were made in solutions of 1 N.KCl pH 2.0 and 1 N.K_2SO_4 pH 2.0 in a similar fashion to section 4.3.1 with the expected result that hydrogen ion was more easily discharged from solutions of pH 2.0 than solutions of pH 3.2, viz. i_o is significantly larger. Best estimates obtained were $i_{oc} = 9.8 \times 10^{-6}$, $\alpha = .183$ in the chloride solution and $i_{oc} = 6.2 \times 10^{-5}$, $\alpha = .162$ in the sulphate solution. However, the validity of these figures is doubtful as it was difficult to polarise the electrodes in these solutions to potentials much more negative than the expected reversible potential of aluminium. It was therefore possible that aluminium was ionising and adding to the current impressed. The difficulty of polarisation is in agreement with the higher values of i_{oc} obtained and if aluminium ionisation was assisting the impressed current, then the true values of i_{oc} will be even higher (true values of α lower) as can be seen from Fig. 29.

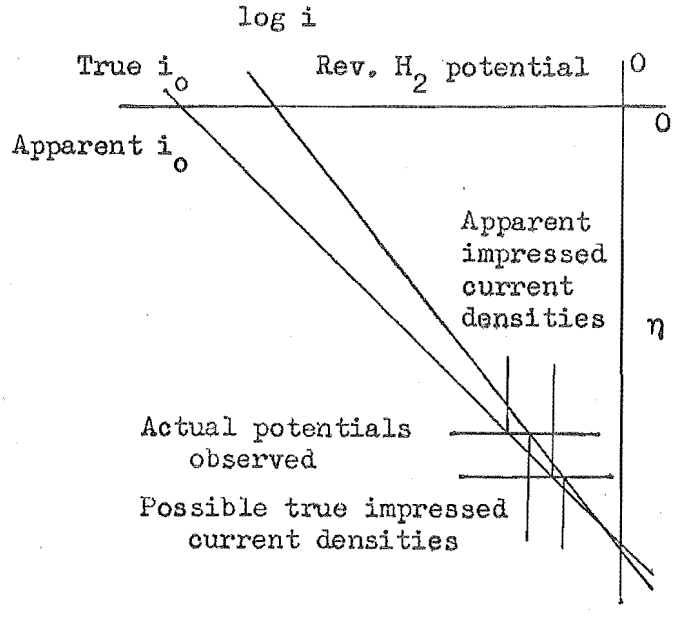

Fig. 29. Effect of aluminium ionisation assisting impressed current on i_{oc} and α_c.

This strong dependence of i_o on pH points to the primary discharge step, i.e. the charge transfer step, as being the controlling step in the overall discharge reaction.

The higher values of i_{oc} in solutions of lower pH obtained here are in agreement with the no-load traces obtained previously by Hagyard

and Williams[7] where a much faster decay to the mixed potential was observed, cf. observations in sulphate (section 4.5.2).

5. CONCLUSIONS

A square wave current method has been used successfully to obtain the cathodic overvoltage parameters for hydrogen evolution on aluminium but found inadequate by itself for determining the anodic parameters for aluminium dissolution, mainly because of the complicating effects of solution IR drop. However, a method was developed for the determination of α_a and the ratio C/i_{oa} from the analysis of the initial potential fall in the 20 μsecs during and just after cutting. By combining these results with the square wave results, it was found possible to obtain the IR drop and i_{oa} and hence C from C/i_{oa}.

It is shown that the no-load peak potential trace obtained cannot be explained unless there is a change in parameters or area function with time. It was found that the more convenient way of expressing this change with time was with the changeover in area function. Whether this concept is real or not in the physical sense is not known for as yet, no visual microscopic evidence for discrete anodic and cathodic areas has been obtained. Even though a simple calculation shows that a single discrete anode on an unloaded electrode after minutes in solution at the mixed potential should be within the resolution of a good optical microscope, this is not so if there are quite a number of anodes (say 100). Thus whether the anodic and cathodic areas are discrete or not is not resolved. If they are discrete the area changeover concept is directly applicable; if they are not the area changeover concept is still applicable theoretically but, when thought of practically, results in a rather complicated concurrent change in i_o for both the cathodic and anodic processes; roughly i_{oc} must increase and i_{oa} decrease with time in a manner similar to that given by the area

ratio changeover.

In aqueous solutions the decay from peak to mixed potentials seems determined by the double layer capacity C and i_{oc}. This is most easily seen by comparing the potential decay from peak to mixed potentials for a normal calculated no-load curve (T.C. of changeover 0.2 ms or faster) with the potential decay through the same potentials obtained by making a step change in current loading for a simple aluminium electrode acting solely as a hydrogen discharging cathode. They are effectively coincident (see Fig. 30). This means that the area changeover or change in parameter, occurs rapidly enough not to control the potential decay.

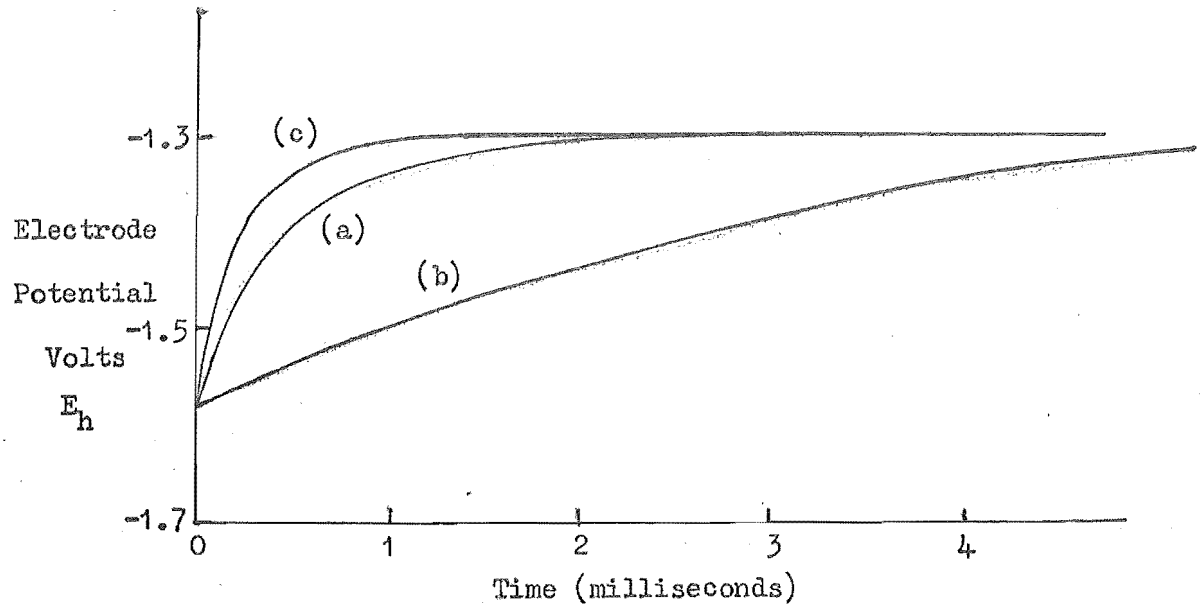

Fig. 30. (a) Potential time curves; predicted no-load curve and predicted potential rise with appropriate step change in cathodic loading; these are coincident.
(b) Actual no-load methanol trace.
(c) Predicted methanol trace if area ratio changed over as rapidly as in aqueous solutions.

In the case of the methanol solution it seems that the decay in potential is controlled by the changeover in area function, thus lending support to the idea that the area ratio change is due to re-orientation of solvent molecules on the electrode surface. An actual methanol potential curve is plotted and compared with that expected if changeover of area occurred as rapidly as in aqueous solutions (see Fig. 30 on previous page).

Cathodic measurements in sulphate show that at potentials more positive than -1.7 volts, hydrogen appears to be more easily discharged from sulphate than chloride solutions of the same pH. The most likely explanation for this seems to be that specific adsorption of chloride ion hinders hydrogen discharge in the latter solution.

6. SYMBOLS

b	slope of Tafel line	
i	impressed current density: cathodic if positive, anodic if negative	(amps/cm^2)
ic	capacitive current density	(amps/cm^2)
i_f	faradaic current density	(amps/cm^2)
i_o	exchange current density	(amps/cm^2)
n	number of electrons transferred in the cathodic rate-controlling process	
r	cathodic to anodic area ratio	
y	ln i	
z	number of electrons transferred in the anodic rate-controlling process	
C	electrical double-layer capacity	(farads/cm^2)
E_h	potential of the electrode on the hydrogen scale	(volts)
E_o	reversible potential of the electrode with respect to the same reference electrode as V	(volts)
F	Faraday	(coulombs)
K	ln i_o	
R	universal gas constant	(joules/$^\circ$K)
R	resistance of solution	(ohms cm^2)
T	absolute temperature	($^\circ$K)
U	apparent overvoltage = η - iR	(volts)
V	potential of the electrode with respect to a reference electrode	(volts)

α overall transfer coefficient

β electron transfer coefficient $(0 < \beta < 1)$

η overvoltage $= V - E_o$

Subscripts

a anodic

c cathodic

7. REFERENCES

1. Clark and Akimov, Compt. Rend. acad. sci., URSS, 30, 805-9 (1941)
2. Brown and Mears, Trans. Electrochem. Soc., 74, 495 (1938)
3. Morise and Lacombe, Compt. Rend., 222, 658-9 (1946)
4. Masing and Altenpohl, Z. Metallkunde, 43, 404 (1952)
5. Chandron, Lacombe and Youssov, Compt. Rend., 229, 201 (1949)
6. Ergang, Masing and Mohling, Z. Electrochem., 55, 160 (1951)
7. Hagyard and Williams, Trans. Far. Soc., 57, 2288 (1961)
8. Earl, B.E.(Hons) Thesis, Univ. of Canterbury (1960)
9. Hagyard and Chapman, in press.
10. Smithells, "Metals reference book", 294, Butterworths (1962)
11. Frumkin, Doln and Ershler, Acta Phys. Chim. URSS, 13, 793 (1940)
12. Randles, Disc. Far. Soc., 1, 11 (1943)
13. Gerischer, Z. Phys. Chem., 198, 286 (1951)
14. Delahay, "New Instrumental Methods in Electrochemistry," Interscience, N.Y.
15. Vielstich and Delahay, J.A.C.S., 79, 1874 (1957)
16. Gerischer and Stanbach, Z. Electrochem., 61, 789 (1957)
17. Barker, Trans. Symp. Electrode Processes, Yeager Ed., 325, Wiley(1961)
18. Sand, Phil. Mag., 1, 45 (1901)
19. Karaoglanoff, Z. Electrochim., 12, 5 (1906)
20. Rojter, Juza and Polujan, Acta Phys. URSS, 10, 389, 845 (1939)
21. Wijnan and Smit, Recuil., 79, 22 (1960)
22. Gerischer, Z. Electrochim., 59, 604 (1955)
23. Berzins and Delahay, J.A.C.S., 77, 6448 (1955)
24. Bockris, "Modern Aspects of Electrochemistry," 180, Butterworths (1954)

25. Karasyk, Law and Linford, J. Electrochem. Soc., 111, 237 (1964)

26. Gill, Proc. Camb. Phil. Soc., 47, 96 (1950)

27. Bass, Proc. Roy Soc., 151, 125 (1964)

28. Watson, Dept Chemical Eng'g, Univ. of Canty, Private communication.

29. Hagyard and Earl, in press.

30. Latimer, "Oxidation Potentials", 263, Prentice-Hall

31. Delahay, Rec. Chem. Prog., 19, 38 (1958)

32. Reilly and Strum, "Progress in Polarography", 1, 81, Interscience, N.Y. (1962)

33. Frumkin, Nikololayora-Fedorovich, Ivanova, Can. J. Chem., 37, 253 (1959)

34. Kolotyrkin, Trans. Symp. Electrode Processes, 191 (1961)

35. Grahame, Chem. Revs., 41, 441 (1947)

36. Bockris, Proceedings 1st Australian Conf. on Electrochem., 705, Pergamon (1965)

37. Kolotyrkin, C.I.T.C.E. 9th meeting, 406, Butterworths, London (1959)

38. Barker, Trans. Symp. Electrode Processes, Yeager Ed., 336, Wiley(1961)

39. Wakelin, M.E. Thesis, Dept. Chemical Eng'g, Univ. of Canty (1964)

40. Bockris, Devanathan and Muller, Proceedings 1st Australian Conf. on Electrochem., 832, Pergamon (1965)

41. Bockris and Potter, J.E.S., 99, 169 (1952)

42. Bockris and Parsons, Trans. Far. Soc., 45, 916 (1949)

8. APPENDICES

8.1 Program I: IBM 1620 Computer Program solving Equations 3 and 7

Considerable effort was devoted to obtaining a general method of solving equations 3 and 7 (p.8 and 10 resp.) and, although a three-point Simpson type integration (stepwise in voltage) proved satisfactory for conditions where no overshoot exists, this method was not suitable for the overshoot cases (i.e. cases with changing area ratio or changing parameters) where the integration must proceed stepwise in time.

Thus a Runge-Kutta method developed by Gill[26] was programmed and with modifications proved very versatile, not only enabling the solution of the equations above but also handling the more complex cases of resistance in parallel or series with either one or both processes.

A Bolzano-type method was used for solving the steady-state equations (implicit in overvoltage) for potential at a given current density. This section of the program could be used in fact for plotting polarisation plots for any polyelectrode system given α's, i_o's and C.

The basic layout and function of the program is most easily seen from the block diagram below. Further detail within any given block can be obtained by referring to the program listing which follows the block diagram. Operating and detailed instructions for input preparation, including format, are available from the complete program write-up in the Department of Chemical Engineering, University of Canterbury.

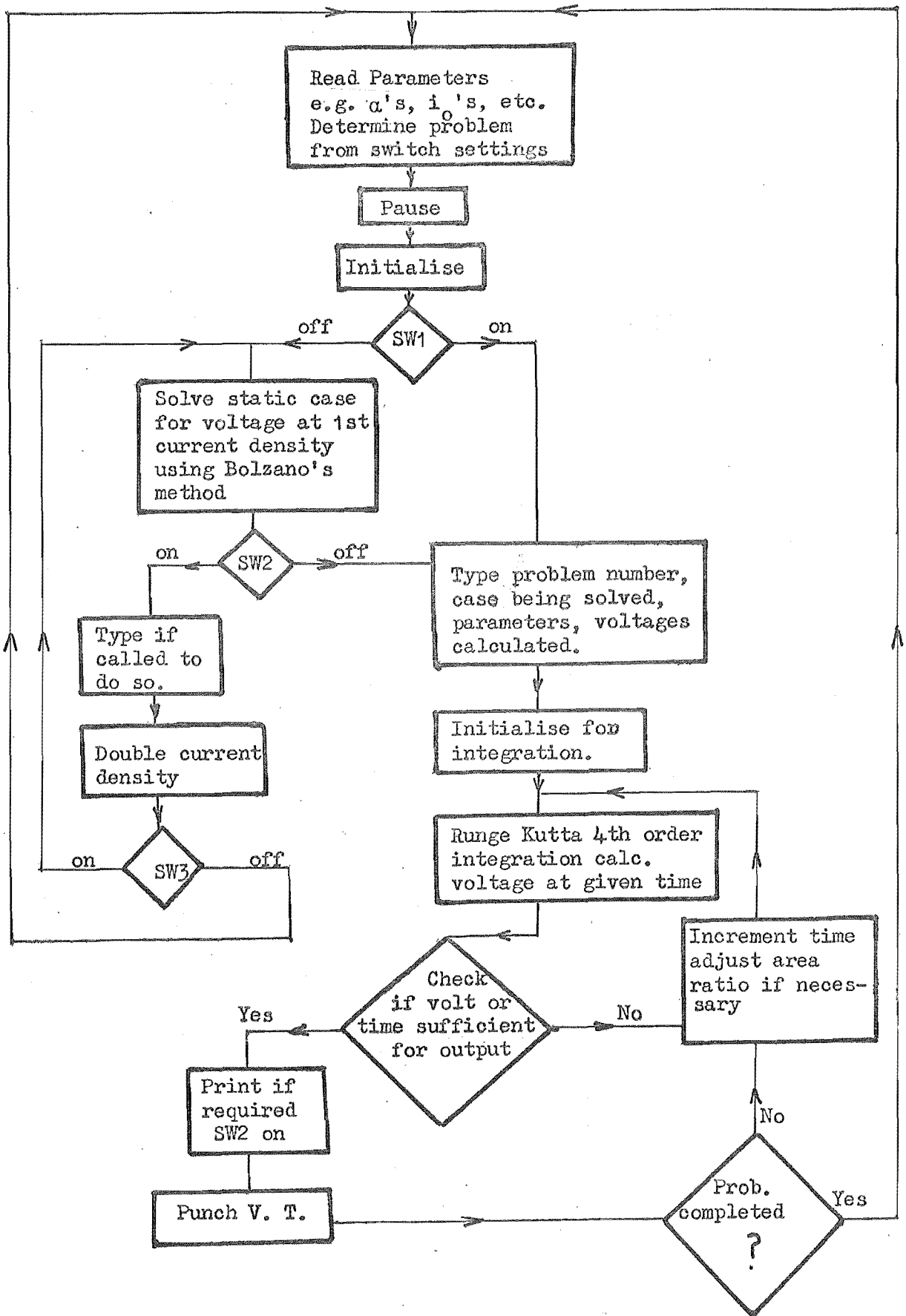

Block Diagram for Program I

```
    DIMENSION B(4),C,4),P(4)
  1 READ2,AI,AII,R,F,D,DI,AL,BL,A,AN,RAP,RCP,ARO
    READ2,BB,XH,V,XT,BYX,BYY,XX
    X=39.4349
    N=1
    M=1
    IF(SENSE SWITCH 1)3,4
  3 M=M+1
  4 IF(SENSE SWITCH 2)5,6
  5 M=M+2
  6 IF(SENSE SWITCH 3)7,8
  7 N=N+1
  8 IF(SENSE SWITCH 4)9,10
  9 N=N+2
 10 PAUSE
    VI=V
 11 RAA=1./(1.+ARO)
    RAC=ARO*RAA
    ZG=A*39.4349
    G=AL*ZG
    GA=(1.-AL)*ZG
    ZG=AN*39.4349
    GB=BL*ZG
    GC=(1.-BL)*ZG
    IF(SENSE SWITCH 1)49,12
 12 ZG=AI
    L=1
 13 J=1
    I=1
 14 AOV=V-RAP
    COV=V-RCP
    IF(M-2)15,16,15
 16 COV=COV+R*ZG
    AOV=AOV+R*ZG
 15 FV=D*(EXP(-G*COV)-EXP(GA*COV))
    GO TO (17,95,19,20),N
 95 IF(M-2)18,19,96
 96 EE=V-R*ZG
    GO TO 19
 20 GO TO (21,17,17,21),M
 21 AOV=AOV+R*(ZG-FV)
 19 FV=FV*RAC+RAA*DI*(EXP(-GB*AOV)-EXP(GC*AOV))
    IF(M-3)17,18,17
 18 FV=FV-V/R
 17 IF(ZG*1.E-5-FV+ZG)22,23,24
 24 IF(ZG*1.E-5+FV-ZG)25,23,23
 22 VN=V
    J=2
    IF(I-2)26,27,27
 26 V=V+.2
    GO TO 14
 25 VP=V
    I=2
    IF(J-2)28,27,27
 28 V=V-.2
```

```
   GO TO 14
27 V=(VN+VP)/2.
   IF(X-FV)29,30,29
29 X=FV
   GO TO 14
30 TYPE40,ZG,FV
23 IF(SENSE SWITCH 2)41,42
41 IF(L-2)43,44,44
43 TYPE2
   TYPE52,M,N,R,F,AL,BL,D,DI
   L=2
   IF(SENSE SWITCH 1)45,44
45 PUNCH100,ZG,V
44 TYPE40,ZG,V
47 ZG=ZG*2.
   IF(SENSE SWITCH 3)13,1
42 IF(L-2)48,12,49
48 VI=V
   L=3
   ZG=AII
   GO TO 13
49 TYPE2
   TYPE71,M,N,AI,VI,AII,V,R,F,D,DI,AL,BL,A,AN,RAP,RCP,ARO
51 V=VI
   A=BB
   TZ=0.
   T=0.
   Q=0.
   B(1)=.5
   B(2)=.29289322
   B(3)=1.7071068
   B(4)=.16666667
   C(1)=.5
   C(2)=B(2)
   C(3)=B(3)
   C(4)=.5
   P(1)=2.
   P(2)=1.
   P(3)=1.
   XXT=XT
   P(4)=2.
   GO TO 88
53 CALL DIO(DI,ARO,TZ,BYX,BYY,RAA,RAC,XH,F)
91 DO541=1,4
   AOV=V-RAP
   COV=V-RCP
   ZF=F
   IF(M-2)55,56,93
93 IF(N-2)55,94,55
94 ZG=(V-EE)/R-AII
   GO TO 62
56 AOV=AOV+R*AII
   COV=COV+R*AII
55 ZG=D*(EXP(-G*COV)-EXP(GA*COV))-AII
   GO TO (57,58,59,60),N
```

```
60 IF(M-2)59,61,59
58 IF(M-2)97,59,97
97 ZG=ZG+V/R
   GO TO 62
57 IF(M-3)62,63,64
63 ZF=ZF-F*R*D*(G*EXP(-G*COV)+GA*EXP(GA*COV))
   GO TO (62,64,62,65),M
65 ZF=(ZF-F)*RAC+F
   ZF=ZF-RAA*DI*R*F*(GB*EXP(-GB*AOV)-GC*EXP(GC*AOV))
   GO TO 62
59 ZG=(AII+ZG)*RAC-AII+RAA*DI*(EXP(-GB*AOV)-EXP(GC*AOV))
   IF(N-3)61,66,67
61 AL=BL
   BL=ZG
   COV=V-RCP-R*(AII+ZG)
   AOV=V-RAP-R*(AII+ZG)
99 IF(BL*1.E-5-AL+BL)55,62,98
98 IF(BL*1.E-5+AL-BL)55,62,62
68 AL=BL
   BL=ZG
   AOV=V-RAP-R*(AII+ZG-D*RAC*(EXP(-G*COV)-EXP(GA*COV)))
   GO TO 99
66 IF(M-3)62,58,63
67 GO TO (63,64,64,68),M
62 ZG=ZG*XH/ZF
   W=B(I)*(ZG-P(I)*Q)
50 V=V+W
54 Q=Q+3.*W-C(I)*ZG
   T=T+XH
74 IF(T-XXT)84,85,85
85 XXT=XXT+XT
88 IF(SENSE SWITCH 2)77,79
77 TYPE80,T,V
   IF(SENSE SWITCH 2)79,81
79 PUNCH100,T,V
81 IF(SENSE SWITCH 4)1,89
89 IF(T-A)53,83,83
84 IF(V-VI-XX)86,87,87
86 IF(VI-V-XX)53,87,87
87 VI=V
   GO TO 88
83 A=A+BB
   CBC=AII
   AII=AI
   AI=CBC
   VI=V
   GO TO 53
 2 FORMAT(4H     6E6.2,2F5.3,2F3.0,2F5.3,E6.3)
52 FORMAT(2I4,3X,2E9.2,2F8.3,3X,2E9.2)
70 FORMAT(4E5.1)
40 FORMAT(E9.2,3X,E9.2)
71 FORMAT(2I4,E9.2,F7.3/8X,E9.2,F7.3,3X,4E9.2/4F8.3,2F6.2,E9.2)
100 FORMAT(2E14.7)
80 FORMAT(E9.2,F8.3,F10.7)
   END
```

8.2 Proof that Overshoot is not possible without Change in 'Constant' Parameters (α, i_o, etc) or area ratio

Overshoot

It is shown below that overshoot is not possible for equation 3 for a step change in polarising current, i, if all parameters other than η and time remain constant from the time of the step change.

From equation 3, page 8

$$\frac{d\eta_c}{dt} = \frac{i - i_{oc}\left(e^{-\frac{\beta nF\eta_c}{RT}} - e^{\frac{(1-\beta)nF\eta_c}{RT}}\right)}{C}$$

Plotting a phase plane diagram ($\frac{d\eta_c}{dt}$ v η_c) for a sudden increase (say) in i, then a figure such as below is obtained and it can quickly be seen that for overshoot to exist the phase plane locus must enter the first quadrant (i.e. $\frac{d\eta_c}{dt}$ must be positive for positive values of $(\eta_c - \eta_{c\ final})$). However, for all positive values of $(\eta_c - \eta_{c\ final})$ $\frac{d\eta_c}{dt}$ is negative (i.e. phase plane locus appears in the 4th quadrant) thus excluding the above condition for overshoot.

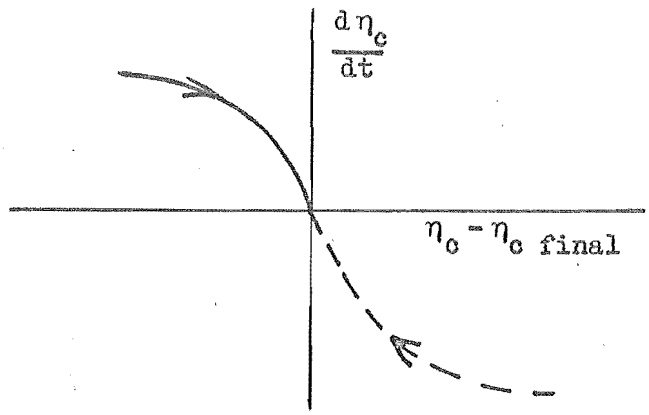

The same argument above applies to the case of the electrode on first cutting when its initial potential is different from its final potential. The dotted curve shown in the 4th quadrant is in fact the locus that would be obtained for a sudden decrease in i.

Except for the change in current involved, the same situation exists when equation 3 is extended to the case of two processes, i.e. equation 7.

8.3 Program II: IBM 1620 Program Computing i_o, α and C

This simple program was written to enable an estimate of the error in α and i_o due to measurement from the photographic traces to be calculated easily and accurately. It also computed 90% confidence values for α and i_o for a series of runs as well as making a correction for IR drop in the solution adjacent to the electrode. (Details in main text, p.39.) The significance of the program variables is given below and the program listing follows. Operating and input specification details are available from the complete write-up in the Department of Chemical Engineering, University of Canterbury.

VP potential of positive flat on electrode potential waveform

VN potential of negative flat on electrode potential waveform

G and B length and breadth of electrode

D length of flat on tip of chisel electrode-cutter

AA angle of cutter

CDI,CDII current densities for respective flats

RI current calibration resistance

AR area of electrode

ALFA α, the transfer coefficient

CAP C, double-layer capacitance

ZIO i_o, the exchange current density

ALM, ZIOM respectively best estimate of α and i_o from a series of runs

ALMI, ALMA 90% confidence limits on α

ZIM, ZAM 90% confidence limits on i_o

AN the number of runs in the series

AV, W, X, Y, Z, A measurements from photographic traces

VR reversible potential of electrode process concerned on calomel scale

The remaining variables in the program are internally necessary and may not have any physical significance.

```
      DIMENSIONEX(3),VP(3),VN(3),VV(3),V(3),VPN(3)
      DIMENSIONCDI(3),CDII(3),CAP(3)
      DIMENSIONALFA(3),ZIO(3),VXX(3)
   22 AN=0.
      SAL=0.
      SALL=0.
      SIOI=0.
      SIO=0.
    1 READ2,B,G,D,AA,RI,AV,W,X,Y,Z,A,VR,TF,DF,DP,VX,EXX,RH,N
      AR=0.01*B*(D+(G-D)/SIN(AA*.008727))
      DO5I=1,3
      EI=I
      EX(I)=EXX*(EI-2.)
      WEX=(W-EX(I))/1.0183
      VP(I)=(A+EX(I))/WEX+1.0183
      VN(I)=(Z+EX(I))/WEX+1.0183
      VV(I)=(VX+EX(I))/WEX
    5 V(I)=AV+EX(I)
      P=1.
      H=1.
      R=[illegible]*(0.08/SQR(AR)-0.2)*360./AA
      DO7I=1,3
      K=4-I
      VCD=[illegible].0183/RI/AR/V(K)
      VEX=V(K)+EX(K)
      VEY=V(I)+EX(I)
      CDII(I)=(Y+VEY)*VCD
      CDI(K)=(X+VEX)*VCD
      RDRI=R*AR*CDII(I)
      RDRK=R*AR*CDI(K)
      VP(I)=VP(I)-RDRI
      VN(K)=VN(K)-RDRK
      IF(SENSE SWITCH 2)14,7
   14 IF(I-2)7,16,7
   16 TYPE17,RDRK,RDRI
    7 VPN(I)=VP(I)-VN(K)
      IF(CDI(1))10,11,11
   10 H=-1.
   11 IF(CDII(1))12,13,13
   12 P=-1.
   13 DO8I=1,3
      K=4-I
      CAP(I)=(CDII(I)-CDI(K  ))*(DP+EX(I))*TF/(DF-EX(I))/VV(K)
      ALFA(I)=.025608*LOG(H*CDI(I)/P/CDII(K))/VPN(K)
      VXX(I)=VN(I)+.025608*LOG(CDI(I)*H)/ALFA(I)
      VPP=(VR-VP(K))/VPN(K)
    8 ZIO(I)=((P*CDII(I))**((VN(I)-VR)/(VP(K)-VR))/(H*CDI(K)))**VPP
      TYPE2
      TYPE6,CDI(2),VN(2),CDII(2),VP(2),AR,CAP(2),ZIO(2),ALFA(2)
```

```
      AN=AN+1.
      A=ALFA(2)
      Z=LOG(ZIO(2))
      SAL=SAL+A
      SALL=SALL+A*A
      SIO=SIO+Z
      SIOI=SIOI+Z*Z
      IF(SENSE SWITCH 3)20,21
   20 ALM=SAL/AN
      W=SQR((SALL-SAL*ALM)/AN)
      Y=SIO/AN
      B=SQR((SIOI-SIO*Y)/AN)
      ZIOM=EXP(Y)
      IF(N-1)24,25,26
   24 ABC=1.65
      GO TO 27
   25 ABC=1.96
   27 ZAM=EXP(Y+ABC*B)
      ZIM=EXP(Y-ABC*B)
      ALMI=ALM-ABC*W
      ALMA=ALM+ABC*W
      TYPE23,ALMI,ALM,ALMA,ZIM,ZIOM,ZAM
   21 IF(SENSE SWITCH 1)4,28
   26 ABC=2.33
      GO TO 27
    4 DO9I=1,3,2
    9 TYPE6,CDI(I),VN(I),CDII(I),VP(I),VXX(I),CAP(I),ZIO(I),ALFA(I)
   28 TYPE 29
      IF(SENSE SWITCH 4)22,1
    2 FORMAT(10HXX JKLM ZZ3F3.2,F3.0,F7.0,7F4.2,E5.2,4F3.2,F4.2,I1)
    6 FORMAT(E9.2,F8.3,3X,E9.2,F8.3,F9.6,3X,E9.2,3X,E9.2,F8.3)
   17 FORMAT(2F6.4)
   23 FORMAT(3F7.3,3(2X,E9.2)/)
   29 FORMAT(//)
      END
```

8.4 Program III: Calculation of α_a and C/i_{oa}

This program was written to calculate the parameters α_a and C/i_{oa} in equation 8 (p.33) by a "hill-climbing" regression analysis using the values and time taken from the no-load electrode potential curve obtained during and just after cutting (see Fig. 17, p.34). The block diagram below shows the overall steps involved and further details can be obtained from the program listing which follows it. As with previous programs operating details, etc, can be obtained from the program write-up available in the Department of Chemical Engineering, University of Canterbury.

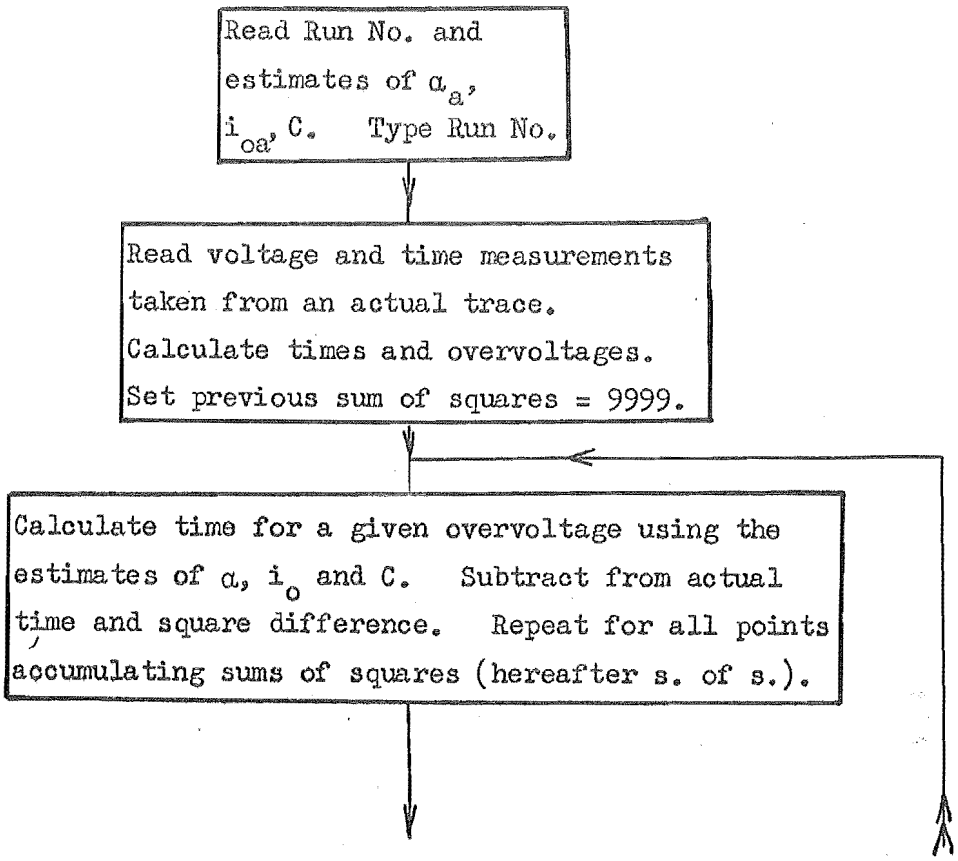

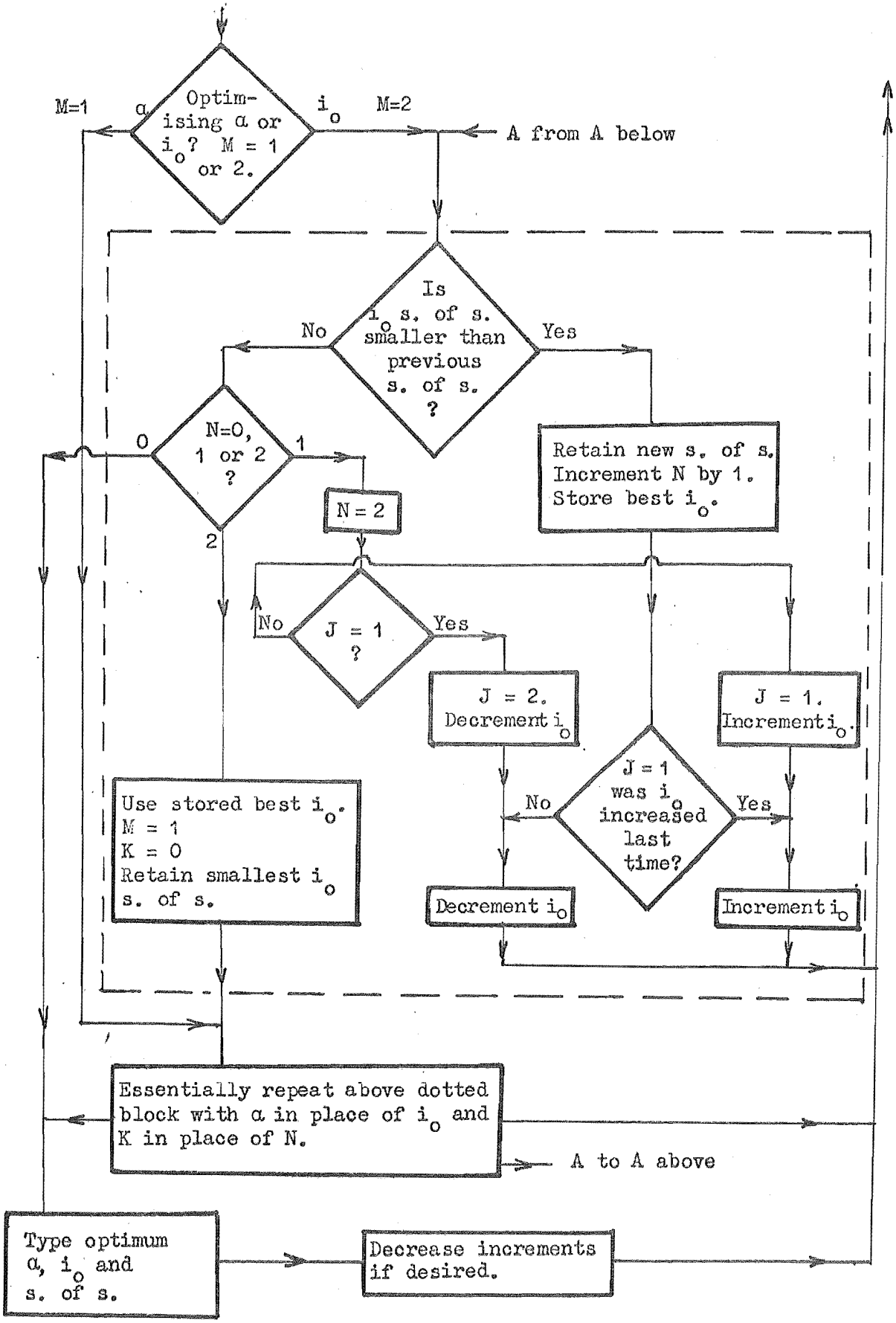

Block Diagram for Program III

```
    DIMENSION V(30),T(30)
21  READ14,AL,VVR,PCAL,DSC,DTS,TPC,ZI,C
    TYPE14
62  I=0
    IF(SENSE SWITCH 2)30,31
30  PUNCH14
31  READ95,XV,XT,J
    IF(J-1)33,34,34
33  X=-XV/DSC*1.0183+PCAL
    I=I+1
    V(I)=X-VVR
    TX=XT/DTS*TPC
    IF(I-1)64,64,63
64  TA=TX
63  T(I)=TX-TA
    IF(SENSE SWITCH 2)18,31
18  PUNCH19,T(I),X
    GO TO 31
34  EX=.02
    EY=.1
    MM=I
    IF(SENSE SWITCH 4)61,57
61  VVR=X
    TYPE20,X
    GO TO 62
57  XD=9999.
    XXD=9999.
    XX=9999.
    M=2
    N=0
12  L=1
    K=0
    J=1
 6  SUMD=0.
    BAL=AL*39.4349
    EJ=EXP( -BAL*V(1))
    CJ=C/BAL/ZI
    DO11I=2,MM
    TD=CJ*(EXP(-BAL*V(I))-EJ)
 1  SUMD=SUMD+(TD-T(I))*(TD-T(I))
    IF(SENSE SWITCH 1)16,67
16  TYPE20,AL,ZI,SUMD
67  IF(M-1)56,56,17
54  ZI=ZIM
    IF(SENSE SWITCH 3)70,71
70  N=0
    IF(XXD-XX)72,74,74
72  XX=XXD
    XXD=9999.
    ZAM=ZI
    GO TO 73
74  XXD=9999.
```

```
    SUMD=XX
    ZI=ZAM
    GO TO 2
71  M=1
    K=0
    SUMD=XXD
56  IF(SUMD-XD)3,2,2
 3  XD=SUMD
73  ALM=AL
    K=K+1
    IF(L-1)4,4,46
51  L=1
    AL=AL+EX
 4  AL=AL+EX
    GO TO 6
 2  IF(K-1)11,50,52
50  K=2
    IF(L-1)25,25,51
25  L=2
    AL=AL-EX
46  AL=AL-EX
    GO TO 6
52  IF(SENSE SWITCH 3)81,76
76  M=2
    N=0
    AL=ALM
    SUMD=XD
17  IF(SUMD-XXD)8,9,9
 8  XXD=SUMD
    N=N+1
    ZIM=ZI
    IF(J-1)10,10,13
 9  IF(N-1)11,53,54
53  N=2
    IF(J-1)41,41,55
55  J=1
    ZI=ZI*(1.+EY)
10  ZI=ZI*(1.+EY)
    GO TO 6
41  J=2
    ZI=ZI*(1.-EY)
13  ZI=ZI*(1.-EY)
    GO TO 6
81  AL=ALM
11  TYPE20,AL,ZI,SUMD
    ACCEPT60,EX,EY
    GO TO 57
14  FORMAT(10HABCDEFGHIJ5F5.3,3E6.2)
19  FORMAT(2E14.7)
20  FORMAT(F6.3,2(3X,E9.2))
95  FORMAT(2F6.3,I2)
60  FORMAT(F4.3,F3.2)
    END
```